Geol. Mag. **154** (*1*), *2017, pp. 96–118.* © *Cambridge University Press 2016*
doi:10.1017/S001675681500093X

Peridotites and basaltic rocks within an ophiolitic mélange from the SW igneous province of Puerto Rico: relation to the evolution of the Caribbean Plate

NADJA OMARA CINTRON FRANQUI*, SUNG HI CHOI*† & DER-CHUEN LEE‡

*Department of Geology and Earth Environmental Sciences, Chungnam National University, 99 Daehangno, Yuseong-gu, Daejeon 34134, South Korea
‡Institute of Earth Sciences, Academia Sinica, Nankang, Taipei 11529, Taiwan, ROC

(*Received* 4 August 2015; *accepted* 21 October 2015; *first published online* 2 February 2016)

Abstract – The geology of Puerto Rico is divided into three regions: the north, central and SW igneous provinces. Characterized by its Jurassic ophiolitic mélange basement, lithology of the SW Igneous Province (SIP) is not related to either of the other two provinces. The ophiolitic mélange is exposed in three peridotite belts: Monte del Estado, Rio Guanajibo and Sierra Bermeja. We present geochemical data to identify the tectonic setting of the SIP peridotite formation and its relation to the evolution of the Caribbean Plate. Comparisons of spinel Cr no. (13–21), Mg no. (63.3–69.6) and TiO_2 suggest an abyssal peridotite origin; however, only Sierra Bermeja presents high TiO_2 characteristics of a mid-ocean-ridge-basalt- (MORB-) like melt reaction. Temperatures determined with two-pyroxene geothermometers indicated a cold thermal regime of *c.* 800–1050 °C, with characteristics of large-offset transform fault abyssal peridotites. The geochemistry and Sr–Nd–Hf–Pb isotopic compositions of basalts within the mélange were also analysed. Las Palmas amphibolites exhibited normal-MORB-like rare earth element (REE) and trace-element patterns, whereas metabasalts and Lower Cajul basalts exhibited island-arc tholeiitic-like patterns. Highly radiogenic Sr isotopes (0.70339–0.70562) of the basalts suggest seawater alteration; however, Pb–Pb and Nd–Hf isotope correlations represent the primary compositions of a Pacific/Atlantic MORB source for the amphibolites, metabasalts and Lower Cajul basalts. We propose that the SIP ophiolitic mélange was formed along a large-offset transform fault, which initiated subduction and preserved both proto-Pacific and proto-Caribbean lithospheric mantle. Younger Upper Cajul basalts exhibited enriched-MORB-like geochemical and isotopic signatures, which can be attributed to a tectonized Caribbean ocean plateau.

Keywords: Puerto Rico, ophiolitic mélange, peridotite, basalt, Sr–Nd–Hf–Pb isotopes.

1. Introduction

Peridotites have been extensively studied; they are of great importance because they can provide direct information about the heterogeneity of the mantle composition and also about the geodynamics of the plates above them (Bodinier & Godard, 2003; Pearson, Canil & Shirey, 2004). Tectonically emplaced mantle rocks include orogenic peridotite massifs and ophiolites. Abyssal peridotites are sampled from the oceanic mantle by dredging on the ocean floors (ridge segments or transform fault zones) or recovered from drill cores (e.g. Dick & Bullen, 1984; Karson *et al.* 1997). Orogenic (or alpine) peridotite massifs are generally dispersed ultramafic bodies and are associated with continental rocks (e.g. Bodinier & Godard, 2003). Ophiolites represent slivers of the ancient oceanic lithosphere obducted onto continental or oceanic crust (e.g. Coleman, 1977; Dilek *et al.* 2000). Ophiolitic mantle rocks are sometimes found to be associated with the formation of back-arc (Pearce *et al.* 1981) or forearc setting (Shervais, 2001). Various exposures of peridotite bodies within an ophiolitic mélange have been found in island arcs and continental margins in and around the Caribbean Plate, including the Great Antilles, Costa Rica, Venezuela and Guatemala (e.g. Giunta *et al.* 2002; Choi *et al.* 2007; Denyer & Gazel, 2009; Madrigal *et al.* 2015).

The evolutionary history of the Caribbean Plate is still a topic of great debate with several models (stabilist versus mobilist views; see Donnelly, 1985; Meschede & Frisch, 1998; Pindell *et al.* 2005, 2012) proposed, although the Pacific provenance model is the most widely accepted. This model proposes that what we know today as the thickened Caribbean oceanic floor is a captured piece of the now largely disappeared Farallon Plate which was located in the Pacific Ocean during Late Jurassic time, before it slowly drifted into its present position between North and South America (Burke, Fox & Şengőr, 1978; Duncan & Hargraves, 1984; Denyer & Gazel, 2009; Kerr & Tarney, 2005). It has been proposed that faulting and related subduction processes produced by the drifting of the Caribbean ocean floor stimulated the emplacement of mantle rocks that are

†Author for correspondence: chois@cnu.ac.kr

today exposed in the Caribbean Plate. In the SW Igneous Province (SIP) of Puerto Rico, there is a mélange of serpentinized spinel peridotite. The serpentinite contains an abundance of Jurassic–Cretaceous xenolithic clasts of amphibolites, pillow basalts and pelagic cherts (Mattson, 1960; Mattson & Pessagno, 1979). Marchesi *et al.* (2011) show that the peridotites are fertile abyssal mantle rocks from mid-ocean ridge, which might be a section of ancient Proto-Caribbean lithospheric mantle trapped in a forearc region generated by northwards subduction of the Caribbean Plate beneath the Proto-Caribbean ocean.

Meanwhile, Jolly *et al.* (1998) suggested that the peridotites might be emplaced into the overlying island-arc complex during a slow upwelling that took place during Maastrichtian time and was associated with a crustal extension induced by strike-slip fault movement. Furthermore, Lidiak, Jolly & Dickin (2011) and Laó-Dávila (2014) suggested that the peridotites might be a lithospheric mantle formed in the back-arc region. Based on spatial relations between the pelagic cherts and amphibolites, Schellekens (1998*a*, *b*) suggested that the amphibolites likely represent part of a transform fault on the ocean floor on which the pelagic cherts have been deposited, or the obducted part of a seamount on the ocean floor that was subducted. Meanwhile, they have a geochemistry which is transitional between normal and enriched mid-ocean-ridge basalt (N-MORB and E-MORB) and arc-like (Schellekens, 1998*b*). The mélange-forming processes are therefore not yet fully understood. To better constrain the tectonic evolution of the Caribbean Plate we determined the Sr–Nd–Hf–Pb isotopic compositions, including major- and trace-element concentrations, of the mafic and ultramafic rocks within an ophiolitic mélange from Puerto Rico.

2. General geology

Located in the Caribbean Plate, the smallest and easternmost island of the Greater Antilles archipelago, Puerto Rico, has a complex geology. This might be the result of multiple subduction and collision events, with its history starting at *c.* 195 Ma (Schellekens, 1998*a*, *b*; Smith & Schellekens 1998; Laó-Dávila, 2014) (Fig. 1a). The Greater Antilles were formed during Early Cretaceous time, somewhere in the Pacific Ocean (Schellekens, 1998*a*). The geology of this island arc is preserved in the basement rocks of Puerto Rico, which are classified into three main groups based on lithostratigraphy, petrography and geochemistry: the North Igneous Province (NIP), the Central Igneous Province (CIP) and the SW Igneous Province (SIP) (Schellekens, 1998*a*) (Fig. 1b). In the CIP and NIP, stratified volcanic island-arc rocks indicate that the first volcanic activity took place during Aptian time (*c.* 120 Ma) and continued until middle Eocene time (*c.* 45 Ma); both are the result of the apparent Antillian-type SW-dipping subduction of the adjacent Atlantic Basin (Jolly *et al.* 1998; Jolly, Lidiak & Dickin, 2008*a*, *b*). However, the geology of the SIP shows no relation whatsoever to the origin of the NIP and CIP; it appears to be a totally different island arc whose first volcanic activity took place during Santonian time (*c.* 85 Ma) by NE-dipping Cordilleran-type subduction, before it later collided with the CIP (Schellekens, 1998*a*; Jolly, Schellekens & Dickin, 2007).

The SIP of Puerto Rico is composed primarily of Santonian – middle Eocene stratified island-arc volcanic, sedimentary and subaerial domains (Jolly *et al.* 1998). The SW part comprises pre-arc basement rocks called the Bermeja Complex, which is considered an ophiolite complex comprising serpentinized spinel peridotites. These contain blocks of partially recrystallized radiolarian chert (the Mariquita chert) and altered MORB-like basalts (the Las Palmas amphibolite and metabasalts, and the Cajul basalts), and most of its contacts are faults (Mattson, 1960; Schellekens, 1998*b*) (Fig. 1c). The ophiolite complex is cut by dioritic dykes and sills (the Maguayo Porphyry of 85 Ma; Laó-Dávila, 2014), and unconformably overlain by the Parguera limestone of Campanian age (Mattson, 1960).

The Bermeja Complex crops out in three distinct belts: the Monte del Estado, the Rio Guanajibo and the Sierra Bermeja (Fig. 1c). The Monte del Estado massif, the largest and northernmost belt, consists predominantly of peridotites (Marchesi *et al.* 2011; Laó-Dávila, Llernadi-Román & Anderson, 2012). The middle Rio Guanajibo belt also comprises mainly peridotites (Hess & Otalora, 1964; Roehrig, Laó-Dávila & Wolfe, 2015). The southernmost belt of the Bermeja Complex contains blocks (up to several hundred metres in size) of amphibolite, metabasalt, basalt and chert within the serpentinized peridotite (Mattson, 1960; Schellekens, 1998*b*). Fragments of amphibolite, metabasalt and chert also occur in the Monte del Estado and Rio Guanajibo serpentinite, but much less than in the Sierra Bermeja (Mattson, 1960; Schellekens, 1998*b*; Laó-Dávila, Llernadi-Román & Anderson, 2012). Radiolarian biostratigraphy indicates that the ages of the cherts range from Early Jurassic to mid-Cretaceous (Montgomery, Pessagno & Pindell, 1994). The Cajul basalt is intercalated with the Mariquita chert, indicating its coeval origin (Volckmann, 1984). K–Ar age determinations on hornblende in the amphibolite range over 126–85 Ma, indicating a metamorphism during this period (Cox *et al.* 1977). The age of serpentinized peridotites is unknown. The stratigraphy indicates that the final crustal emplacement of the ophiolitic mélange is Coniacian–Turonian (86–94 Ma) (Laó-Dávila, 2014).

3. Materials and methods

3.a. Petrography

3.a.1. Peridotites

Peridotites were collected from three localities: Monte del Estado, Rio Guanajibo and Sierra Bermeja. They are composed of olivine, orthopyroxene,

https://doi.org/10.1017/S001675681500093X Published online by Cambridge University Press

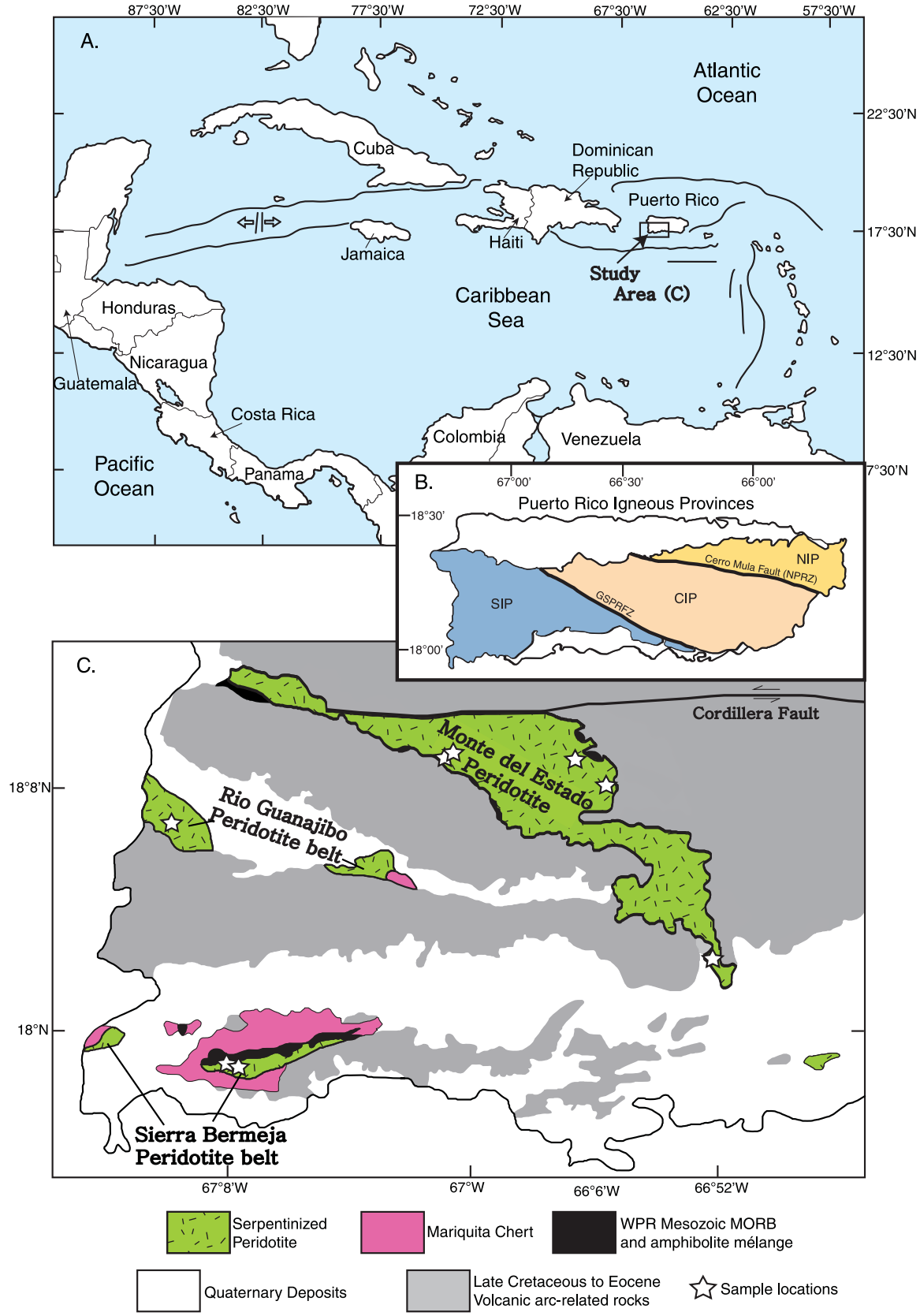

Figure 1. (Colour online) (a) Map of the Caribbean and Central American region. The box shows the location of the study area. (b) Simplified geological map of the igneous provinces of Puerto Rico. NIP – North Igneous Province; CIP – Central Igneous Province; SIP – SW Igneous Province. Modified after Schellekens (1998a). (c) Geological sketch map of the SW block of Puerto Rico with sample locations (stars), after Marchesi *et al.* (2011) and Lidiak, Jolly & Dickin (2011).

https://doi.org/10.1017/S001675681500093X Published online by Cambridge University Press

Table 1. Modal analyses of spinel peridotite bodies from the SW block of Puerto Rico. ND – not determined.

Sample No.	Rock type	Modes (vol %)				% Serpentine
		Olivine	Orthopyroxene	Clinopyroxene	Spinel	
Monte del Estado						
PRME01	Spinel harzburgite	63.1	35.6	0.9	0.4	84.0
PRME03	Spinel lherzolite	64.4	21.2	12.3	2.1	65.5
PRME05	Spinel lherzolite	68.0	20.0	10.0	2.0	73.2
PRME06	Spinel harzburgite	68.7	30.0	0.8	0.5	91.2
PRME09	Spinel harzburgite	66.4	29.2	3.0	1.4	89.7
Rio Guanajibo						
PRRG-01	Spinel harzburgite	62.0	36.8	0.7	1.2	73.9
Sierra Bermeja						
PRSB01	Spinel peridotite	ND	ND	ND	2.2	97.8
PRSB02	Spinel peridotite	ND	ND	ND	2.7	97.3

clinopyroxene and spinel. Hydrous minerals and garnet are absent. Modal compositions were determined by point-counting (Table 1). The rock types were spinel lherzolites and harzburgites. Lherzolites contain 64–68 % olivine, 20–21 % orthopyroxene, 10–12 % clinopyroxene and 2 % spinel. Harzburgites contain 62–69 % olivine, 30–37 % orthopyroxene, 1–3 % clinopyroxene and 1–3 % spinel. Most of the samples studied were overprinted by the growth of serpentine minerals, which ranged over 66–98 % (Table 1). Some portions of serpentinized peridotites contain fresh relicts of primary minerals; however, only a few spinel relicts are observed in highly (*c.* 98 %) serpentinized Sierra Bermeja peridotites.

3.a.2. Basaltic rocks

Basaltic samples were collected at the Sierra Bermeja Complex located in the south-westernmost part of the SIP. They were classified as the Las Palmas amphibolites (PRAMP02, PRAMP04) and metabasalts (PRAMP01-G, PRAMP03, PRAMP01-V), the Lower Cajul basalts (PRLCJ01, PRLCJ02) and the Upper Cajul basalts (PRNUC01, PRNUC02, PRNUC03). The amphibolites are composed of foliated green-brown hornblende, albite plagioclase and quartz, with relict clinopyroxene also present in sample PRAMP02. The metabasalts have a porphyritic texture with hornblende and plagioclase phenocrysts in a groundmass of the same phases, where chlorite and/or prehnite alteration of the hornblende crystals is also present.

Both the Lower Cajul and Upper Cajul samples are pillow basaltic rocks, and hydrothermal alteration has greatly affected the original mineralogy. The Lower Cajul samples have a porphyritic texture, and plagioclase phenocrysts lie in a plagioclase–clinopyroxene matrix showing an ophitic texture. The clinopyroxenes are altered to green chlorite. Calcitic veinlets crosscut the Upper Cajul samples. In sample PRNUC01, chloritized clinopyroxenes dominated the main mineralogy. Samples PRNUC02 and PRNUC03 had a relatively fresh ophitic texture with some chloritized clinopyroxene phenocrysts.

3.b. Analytical procedures

Mineral compositions were obtained from thin rock sections using a wavelength-dispersive electron microprobe (JXA-8100: JEOL Ltd., Tokyo, Japan) with ZAF matrix correction at the Gyeongsang National University in Jinju, South Korea. The analysis was conducted with an accelerating voltage of 15 kV, beam current of 10 nA, beam diameter of 1 μm, and a counting time of 20 s for each spot. Natural minerals were used as standards for Na, Si, Fe, K, Al, Mn, Ca, Mg, P, Cr and Ti, and a synthetic oxide was used for Ni. All of the mineral analyses reported here represent averages of various analytical targets of each mineral in each sample. The results are listed in online supplementary Table S1 (available at http://journals.cambridge.org/geo). Accurate measurements of the Ca concentration in olivines were made using an accelerating voltage of 20 kV, a beam diameter of 100 nA and a counting time of 100 s. The accuracy of the analysis was 3 % (1σ), with a detection limit of *c.* 20 ppm Ca. The raw data were corrected to a preset olivine matrix (Fo_{90}). The reported CaO values in online Table S1 obtained under these operating conditions represent the average of five rounds of analysis of several grain cores.

Samples for whole-rock analysis were crushed into <0.5 cm pieces in a tungsten carbide mortar and ultrasonically cleaned with milli-Q ultrapure water. Fresh fragments were pulverized with an agate ball mill prior to geochemical analysis. Whole-rock major elements were analysed by X-ray fluorescence spectrometry at the Pukyong National University in Pusan, South Korea. The data were reduced with a weighted regression line created with standards (BIR-1 and MO-5). The precision of the technique for preparing and analysing the standards was within 5 %. The results are given in Tables 2 and 3. Whole-rock trace-element concentrations were determined using inductively coupled plasma mass spectrometry (ICP-MS) at Act Labs, Ontario, Canada. Precision was estimated to be ±10 % based on replicated analyses of international rock standards (BIR-1, JR-1 and DNC-1). The results are presented in Table 3.

The isotope analyses for peridotites were performed on nearly pure clinopyroxene separates to

https://doi.org/10.1017/S001675681500093X Published online by Cambridge University Press

Table 2. Whole-rock major-element contents (wt %) for spinel peridotites from the SW block of Puerto Rico.

Location	Monte del Estado					Rio Guanajibo	Sierra Bermeja	
Sample No.	PRME01	PRME03	PRME05	PRME06	PRME09	PRRG01	PRSB01	PRSB02-A
Rock type	Spinel harzburgite	Spinel lherzolite	Spinel lherzolite	Spinel harzburgite	Spinel harzburgite	Spinel harzburgite	Spinel harzburgite	Spinel harzburgite
GPS position	N18° 9′ 32.04″, W66° 59′ 55.06″	N18° 8′ 46.29″, W66° 57′ 5.40″	N18° 9′ 44.40″, W67° 1′ 55.93″	N18° 9′ 39.11″ W67° 2′ 11.45″	N18° 2′ 13.53″ W66° 53′ 4.77″	N18° 7′ 49.97″ W67° 9′ 33.79″	N17° 59′ 13.26″ W67° 8′ 6.91″	N17° 58′ 59.94″ W67° 8′ 06.47″
SiO_2	39.4	39.0	38.7	37.1	38.1	38.5	38.0	37.6
TiO_2	0.05	0.07	0.05	0.05	0.04	0.05	0.05	0.06
Al_2O	2.13	2.63	2.38	2.11	2.18	2.00	2.43	2.31
Fe_2O_3*	6.97	8.35	8.46	8.93	8.27	8.73	9.17	9.77
MnO	0.15	0.12	0.12	0.15	0.12	0.18	0.12	0.14
MgO	37.0	35.8	36.7	36.4	36.2	35.6	36.0	36.6
CaO	0.69	2.75	2.30	0.11	1.00	0.24	0.22	0.10
Na_2O	0.00	0.00	0.00	0.00	0.00	0.00	0.00	0.00
K_2O	0.02	0.02	0.02	0.02	0.02	0.02	0.03	0.02
P_2O_5	0.00	0.00	0.00	0.00	0.00	0.00	0.00	0.00
LOI	13.8	11.4	11.4	15.3	14.2	14.7	14.1	13.6
Total	100.2	100.2	100.2	100.2	100.2	100.1	100.1	100.1
Mg no.	92.3	90.6	90.7	90.1	90.8	90.2	89.8	89.4

*Total Fe as Fe_2O_3.

avoid the effects of serpentinization and weathering. Clinopyroxene grains were prepared from unweathered samples using nylon sieves for sizing, a magnetic separator to eliminate grains with dark inclusions, and hand-picking under a binocular microscope to select only the optically clear grains for analysis. Prior to dissolution for the isotopic analyses, the minerals were washed in milli-Q ultrapure water in a heated ultrasonic bath for 1 hour. After removing the milli-Q ultrapure water and rinsing the minerals repeatedly, two leaching steps with 2 N HCl and 6 N HCL (30 min at 120 °C) were performed, with a milli-Q rinse after each of these steps. Chemical separations of Sr, Nd, Pb and Hf for clinopyroxenes and basaltic rocks were performed at Chungnam National University in Daejeon, South Korea. The column procedures used for Sr, Nd, Pb and Hf isotopic compositions have been described elsewhere (Mukasa *et al.* 1991; Münker *et al.* 2001). Separation of Sr and Nd was performed following standard ion exchange techniques (Bio-Rad AG50W-X8 for Sr and REEs, HDEHP-coated Teflon for Nd). The separation of Pb and Hf was achieved using Bio-Rad AG1-X8 and EICHROM LN resin chromatography, respectively. The isotopic analyses for Sr, Nd and Pb were performed at the Korea Basic Science Institute using a thermal ionization mass spectrometer (TIMS; VG Sector, VG Analytical, London, UK). The $^{87}Sr/^{86}Sr$ and $^{143}Nd/^{144}Nd$ ratios were corrected for instrumental mass fractionation by normalizing to $^{86}Sr/^{88}Sr = 0.1194$ and $^{146}Nd/^{144}Nd = 0.7219$, respectively. Replicated analyses of NBS-987 and JNdi-1 standards yielded $^{87}Sr/^{86}Sr = 0.710247 \pm 0.000003$ ($N = 10$, 2σ) and $^{143}Nd/^{144}Nd = 0.512102 \pm 0.000004$ ($N = 10$, 2σ). Measured Pb isotopic ratios were corrected for instrumental mass fractionation of 0.1 % amu^{-1} by reference to replicate analyses of the NBS-981 standard. Total blanks averaged 30 pg for Sr and Nd and 50 pg for Pb. The Hf isotopic analyses were conducted using a Neptune mass spectrometer (Thermo Fisher Scientific, Waltham, MA, USA) at the Institute of Earth Sciences, Academia Sinica, in Taipei, Taiwan. To monitor machine performance, the JMC-475 standard was run between study samples. A mean $^{176}Hf/^{177}Hf$ ratio of 0.282149 ± 0.000007 ($N = 20$, 2σ) was obtained, and the values reported were normalized to the accepted value of 0.282160. The total blank level was approximately 30 pg for Hf. The results are reported in Tables 2 and 3.

4. Results

4.a. Peridotites

4.a.1. Mineral chemistry

Spinel: The Monte del Estado and Rio Guanajibo peridotites contain spinels with low Cr numbers (100 Cr/(Cr + Al) = 13.0–21.0) and high Mg numbers (100 Mg/(Mg + Fe) = 67.0–72.4) (online supplementary Table S1, available at http://journals.cambridge.org/geo). The Sierra Bermeja

https://doi.org/10.1017/S001675681500093X Published online by Cambridge University Press

Table 3. Whole-rock major-element contents (wt %) and Sr–Nd–Pb–Hf isotopic composition for basaltic rocks from the Sierra Bermeja Complex, SW block of Puerto Rico. ND – not determined; LOI – loss on ignition.

Sample No.	PRAMP01-G	PRAMP01-V	PRAMP03-V	PRAMP02	PRMAMP04	PRLCJ01	PRLCJ02	PRNUC01	PRNUC02	PRNUC03
Rock type	Metabasalt	Metabasalt	Metabasalt	Amphibolite	Amphibolite	Basalt	Basalt	Basalt	Basalt	Basalt
GPS position	N17° 59′ 1.14″ W67° 8′ 7.15″	N17° 59′ 1.15″ W67° 8′ 7.16″	N17° 58′ 59.88″ W67° 8′ 06.44″	N17° 58′ 59.94″ W67° 8′ 06.47″	N17° 59′ 7.29″ W67° 8′ 03.84″	N17° 58′ 49.95″ W67° 8′ 10.59″	N17° 58′ 50.54″ W67° 8′ 10.81″	N17° 59′ 43.72″ W67° 7′ 49.89″	N17° 59′ 42.31″ W67° 7′ 49.64″	N17° 59′ 44.89″ W67° 7′ 50.10″
Age[a]	185 Ma	185 Ma	185 Ma	185 Ma	185 Ma	185 Ma	185 Ma	85 Ma	85 Ma	85 Ma
Major elements (wt%)										
SiO_2	51.0	51.0	51.2	47.3	49.5	51.8	52.4	48.7	50.6	48.3
TiO_2	1.19	1.03	1.24	2.21	1.98	1.87	1.85	1.91	1.70	1.84
Al_2O	15.7	15.4	15.2	13.1	13.5	12.8	13.3	16.5	15.3	14.1
Fe_2O_3[b]	10.1	9.6	10.4	15.0	13.8	12.1	11.3	11.0	10.8	14.7
MnO	0.16	0.15	0.16	0.23	0.21	0.20	0.17	0.13	0.16	0.20
MgO	6.5	7.1	6.8	7.8	6.9	6.1	6.3	4.6	5.2	5.4
CaO	9.5	9.7	9.6	10.0	9.5	7.5	7.9	5.3	7.0	8.8
Na_2O	3.55	3.23	3.13	2.87	3.32	4.40	3.37	5.76	4.79	3.20
K_2O	0.38	0.56	0.45	0.13	0.09	0.69	0.82	0.33	1.22	0.38
P_2O_5	0.10	0.08	0.11	0.18	0.18	0.15	0.15	0.19	0.18	0.18
LOI	1.62	1.89	1.68	0.86	0.92	2.40	2.47	5.50	2.87	2.94
Total	99.9	99.8	99.9	99.8	99.9	100.0	99.9	99.9	99.9	99.9
Mg no.[d]	59.2	62.5	59.4	53.9	52.8	53.1	55.5	48.6	51.8	45.3
Isotopes										
$^{87}Sr/^{86}Sr$	0.704116	0.704176	0.703825	0.703763	0.703663	0.704485	0.704546	0.705172	0.705800	0.704207
2σ	0.000007	0.000009	0.000009	0.000009	0.000009	0.000010	0.000007	0.000006	0.000007	0.000010
$(^{87}Sr/^{86}Sr)_i$	0.703795	0.703666	0.703386	0.703667	0.703610	0.703835	0.703844	0.705061	0.705616	0.704064
$^{143}Nd/^{144}Nd$	0.513146	0.513145	ND	0.513120	0.513095	0.513098	0.513088	0.512917	0.512917	0.512918
2σ	0.000005	0.000009	ND	0.000004	0.000012	0.000006	0.000006	0.000004	0.000004	0.000005
$(^{143}Nd/^{144}Nd)_i$	0.512881	0.512879	ND	0.512946	0.512829	0.512811	0.512819	0.512822	0.512822	0.512821
ε_{Nd}[c]	9.4	9.3	ND	10.7	8.4	8.0	8.2	5.7	5.7	5.7
$^{176}Hf/^{177}Hf$	0.283207	0.283206	0.283204	0.283330	0.283274	0.283168	0.283161	0.283085	0.283089	0.283045
2σ	0.000005	0.000005	0.000004	0.000007	0.000006	0.000004	0.000004	0.000004	0.000004	0.000004
$(^{176}Hf/^{177}Hf)_i$	0.283100	0.283095	0.283098	0.283219	0.283155	0.283044	0.283044	0.283055	0.283055	0.283011
ε_{Hf}[c]	15.7	15.5	15.6	19.9	17.6	13.7	13.7	11.9	11.9	12.5
$^{206}Pb/^{204}Pb$	18.20	18.09	18.16	18.24	18.34	18.63	18.72	19.33	19.13	19.00
$(^{206}Pb/^{204}Pb)_i$	17.93	17.83	17.92	17.93	18.19	18.28	18.47	18.96	18.74	18.71
$^{207}Pb/^{204}Pb$	15.48	15.49	15.52	15.49	15.49	15.51	15.50	15.62	15.60	15.58
$(^{207}Pb/^{204}Pb)_i$	15.47	15.48	15.50	15.47	15.49	15.49	15.49	15.61	15.58	15.57
$^{208}Pb/^{204}Pb$	37.73	37.68	37.76	37.78	37.86	38.10	38.08	39.04	39.12	38.98
$(^{208}Pb/^{204}Pb)_i$	37.55	37.47	37.61	37.61	37.74	37.77	37.87	38.62	38.37	38.44

[a]Age values as given by Lidiak, Jolly & Dickin (2011).
[b]Total Fe as Fe_2O_3.
[c]ε_{Nd} and ε_{Hf} are calculated via $^{147}Sm/^{144}Nd = 0.1963$, $^{143}Nd/^{144}Nd = 0.512638$, $^{176}Lu/^{177}Hf = 0.0342$, and $^{176}Hf/^{177}Hf = 0.282772$ for present-day chondritic Earth.
[d]Mg no. calculated assuming $Fe_2O_3/FeO = 0.15$.

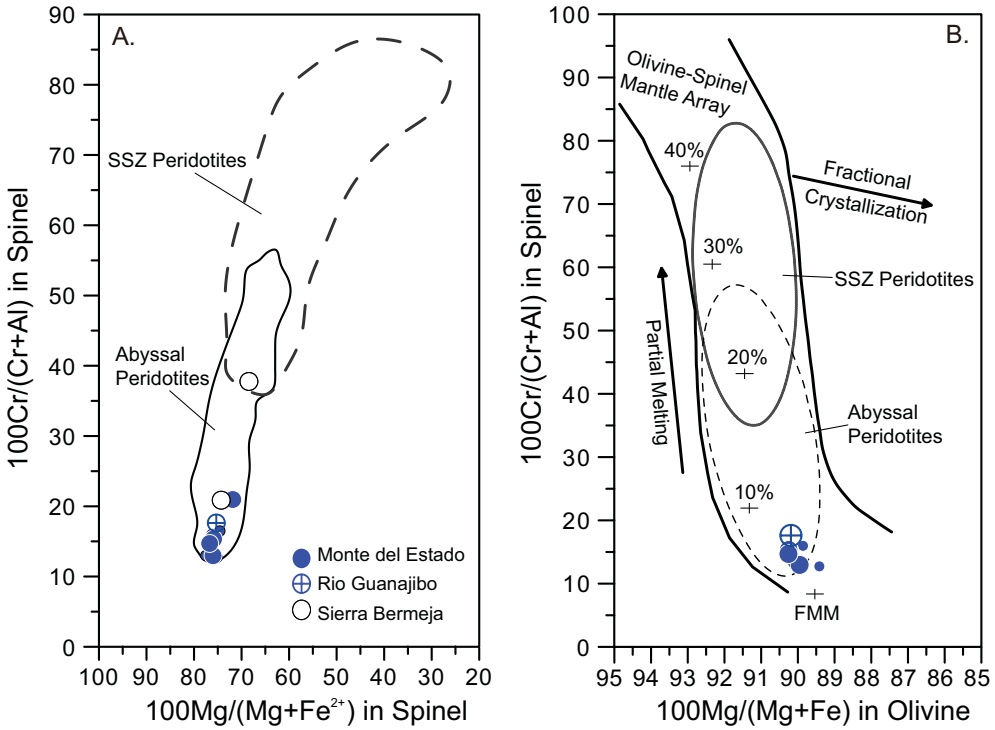

Figure 2. (Colour online) Plots of spinel quad and (a) 100 Cr/(Cr + Al) of spinel and (b) 100 Mg/(Mg + Fe) content of coexisting olivine from Monte del Estado, Rio Guanajibo and Sierra Bermeja peridotites. The ferrous iron content in spinel was calculated on a stoichiometric basis. The olivine–spinel mantle array and melting trend (annotated by melting %) given in (b) are from Arai (1994). Abyssal peridotite and suprasubduction zone (SSZ) peridotite fields are from Dick & Bullen (1984) and Choi *et al.* (2008). Small symbols represent Monte del Estado peridotite data from Marchesi *et al.* (2011). FMM – fertile mantle.

peridotites contain spinels with much higher Cr numbers (20.9–37.8) and lower Mg numbers (63.3–69.6) than the Monte del Estado and Rio Guanajibo peridotites (online Table S1). However, all of the spinels along with literature data for spinels from the Monte del Estado peridotites were plotted within the field of abyssal peridotites (Fig. 2a).

Olivine: Relict olivines (i.e. remaining from the original unserpentinized peridotites) from the Monte del Estado and Rio Guanajibo peridotites range in composition from $Fo_{90.0}$ to $Fo_{90.3}$ (online supplementary Table S1, available at http://journals.cambridge.org/geo), which are within the compositional range of literature data for olivines from the two peridotites (Hess & Otalora, 1964; Marchesi *et al.* 2011). Olivine grains from the Sierra Bermeja peridotites have been totally overprinted by the growth of serpentine minerals. The compositions obtained were plotted in a diagram showing spinel Cr no. versus coexisting olivine Mg no. (Fig. 2b). All of the samples plotted within the olivine–spinel mantle array inside the abyssal peridotite field, indicating that the composition of olivine is correlated with that of spinel.

Pyroxenes: The chemical composition of relict pyroxenes could only be measured for the Monte del Estado and Rio Guanajibo peridotites due to the strong serpentinization of the Sierra Bermeja peridotites. Orthopyroxenes are enstatite, with a composition of $Wo_{1.2–1.5}En_{87.6–89.0}Fs_{9.8–10.8}$ (online supplementary Table S1, available at http://journals.cambridge.org/geo). The Mg numbers ranged over 91.5–93.6. The Al_2O_3 and Cr_2O_3 concentrations ranged over 4.1–4.4 wt % and 0.4–0.8 wt % respectively (Table S1). Clinopyroxenes are diopside, with a composition of $Wo_{45.6–49.6}En_{46.3–49.7}Fs_{3.6–4.9}$ (Table S1). The Mg numbers ranged over 92.7–94.5. The Al_2O_3 and Cr_2O_3 concentrations ranged over 3.6–4.9 wt % and 0.6–0.8 wt %, respectively (Table S1).

4.a.2. *Whole rock*

Whole-rock major-element concentrations for the spinel peridotites studied here are given in Table 2. The Mg numbers varied over the range 89.4–92.3, which is in agreement with the values of previous studies on the Monte del Estado (Mg no. = 89.5–91.4; Marchesi *et al.* 2011) and Rio Guanajibo peridotites (Mg no. = 89.6–91.8; Hess & Otalora, 1964). The CaO and Al_2O_3 concentrations ranged over 0.1–2.8 wt % and 2.0–2.6 wt %, respectively. Average TiO_2 and K_2O values were 0.05 and 0.02 wt %, respectively. Loss on ignition (LOI) values ranged over 11.4–15.3 %. In the plot of MgO/SiO_2 versus Al_2O_3/SiO_2 ratios (Fig. 3), all samples were within the terrestrial mantle array (Jagoutz *et al.* 1979; Hart & Zindler, 1986), indicating that the major-element concentrations were not significantly affected by hydrothermal alteration despite the large degree of serpentinization represented by LOI values and modal analyses (Table 1). The Puerto Rico peridotites had lower Al_2O_3 and higher MgO

https://doi.org/10.1017/S001675681500093X Published online by Cambridge University Press

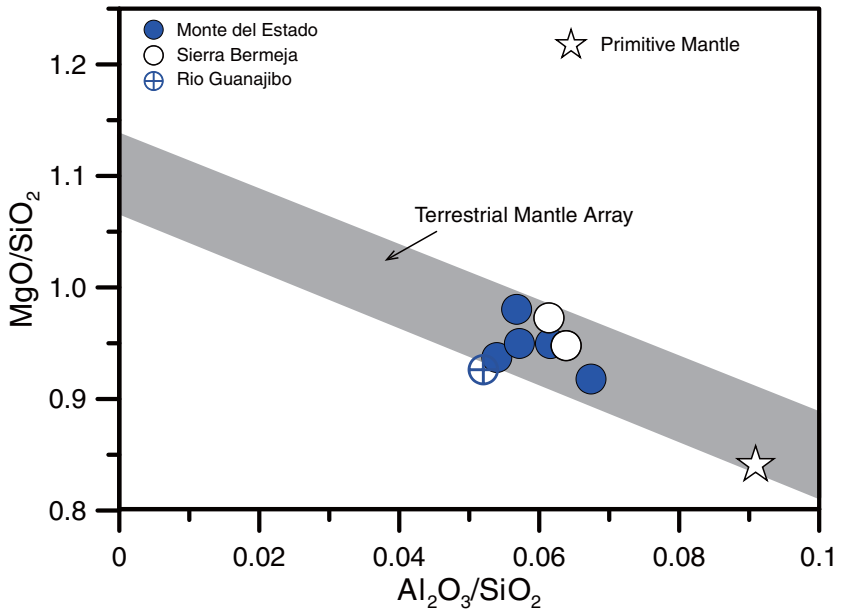

Figure 3. (Colour online) Whole-rock MgO/SiO_2 v. Al_2O_3/SiO_2 ratios for spinel peridotites from the SW block of Puerto Rico. The terrestrial mantle array is from Jagoutz *et al.* (1979) and Hart & Zindler (1986). Primitive mantle compositions are from Wänke (1981).

contents than the primitive mantle composition (Fig. 3), suggesting that they are residues after various degrees of partial melting.

4.a.3. Clinopyroxene isotopes

Clinopyroxenes are major carriers of rare earth elements (REEs) and possibly Hf in the anhydrous spinel peridotite mineral assemblages (e.g. Eggins, Rudnick & McDonough, 1998; Bedini & Bodinier, 1999; Choi *et al.* 2008); we therefore considered the data for this mineral to be representative of each peridotite. The Hf isotopic compositions of clinopyroxenes separated from the Monte del Estado peridotites are given in online supplementary Table S1 (available at http://journals.cambridge.org/geo). The $^{176}Hf/^{177}Hf$ ratios ranged over 0.283418–0.283958 (ε_{Hf} = 22.8–41.9), indicating a time-integrated depleted nature of the peridotites.

4.b. Basaltic rocks

4.b.1. Major and trace elements

Whole-rock major- and trace-element concentrations of the basaltic rocks from the Sierra Bermeja Complex are given in Tables 3 and 4. For the classification, the samples were plotted in a total alkali versus silica diagram (TAS) (Fig. 4). The Las Palmas amphibolites and metabasalts had a subalkaline (tholeiitic) basalt composition. The amphibolites had Mg no. in the range 53.9–52.8 and the metabasalts 62.5–59.2. The Lower Cajul samples were subalkaline basaltic andesites, with Mg no. of 55.5–53.1. The Upper Cajul samples had transitional basalt to basaltic trachyandesite composition, with Mg no. 51.8–45.3. Although the Cajul samples were classified as basalt to basaltic andesites and trachyandesites in Figure 4, we used the commonly accepted terminology of basalts for the samples in this area. The Ni, Co and Cr contents of the basaltic rocks were 60–30, 45–32 and 170–30 ppm, respectively (Table 4). The Mg no. and the Ni and Cr contents of the basaltic rocks were lower than the values observed in primitive basalts (Mg no. >70, Ni >400–500 ppm, Cr >1000 ppm; Frey, Green & Roy, 1978; Wilkinson & Le Maitre, 1987), reflecting olivine ± clinopyroxene fractionation during the magma evolution. Variations in the major oxides are shown in Figure 5. MgO was negatively and positively correlated with CaO and Na_2O, respectively. However, the large intersample variations in SiO_2, TiO_2, Al_2O_3, Fe_2O_3, MnO, K_2O and P_2O_5 could not be explained by simple fractional crystallization of these minerals from a single parent magma; instead, they indicated variable primary magmas.

Chondrite-normalized REE patterns for the Sierra Bermeja basaltic rocks are shown in Figure 6a and b. The amphibolites, metabasalts and Lower Cajul basalts exhibited N-MORB-like light-rare-earth-element- (LREE-) depleted patterns, with $(La/Yb)_N$ in the range 0.4–0.7 and $(Yb)_N$ in the range 14.7–29.4. However, the amphibolites were distinguished from the metabasalts by relatively higher REE abundances and a slight negative Eu anomaly, reflecting plagioclase fractionation. The Lower Cajul basalts had a similar REE pattern to the amphibolites, also with slightly higher abundances in REE than the metabasalts and with a negative Eu anomaly. The Upper Cajul basalts exhibited an E-MORB-like LREE pattern, with a $(La/Yb)_N$ range of 1.9–2.3 and a $(Yb)_N$ range of 15.3–17.1. They did not have a significant Eu anomaly. Primitive mantle-normalized trace-element patterns are shown in Figure 6c and d, revealing a major chemical distinction between metabasalt and amphibolite. The amphibolites

https://doi.org/10.1017/S001675681500093X Published online by Cambridge University Press

Table 4. Trace-element contents (ppm) for basaltic rocks from the Sierra Bermeja Complex, SW block of Puerto Rico.

Sample No.	PRAMP01-G	PRAMP01-V	PRAMP02	PRAMP03-V	PRMAMP04	PRLCJ01	PRLCJ02	PRNUC01	PRNUC02	PRNUC03
Rock type	Metabasalt	Metabasalt	Amphibolite	Metabasalt	Amphibolite	Basalt	Basalt	Basalt	Basalt	Basalt
Ni	50	60	50	60	60	50	40	30	30	30
Co	32	32	45	32	38	40	36	36	39	36
Cr	130	140	110	170	90	110	110	40	40	30
V	284	279	467	301	416	385	379	269	271	345
Cu	80	70	30	70	40	60	50	110	30	80
Zn	70	60	90	70	90	100	90	120	100	100
Ga	16	15	19	16	18	13	15	17	15	19
Cs	<0.5	<0.5	<0.5	<0.5	<0.5	<0.5	<0.5	<0.5	<0.5	<0.5
Ba	247	289	22	392	31	72	85	70	61	71
Rb	7	12	1.1	9	0.7	10	12	6	20	7
Sr	166	179	90	156	99	117	130	189	379	171
Y	25	22	45	26	40	36	37	25	24	28
Zr	65	53	125	71	106	98	98	101	88	104
Nb	1	<1	4	1	3	3	2	11	10	10
Ta	<0.1	<0.1	0.2	<0.1	0.2	0.2	0.2	0.6	0.9	0.7
Hf	1.8	1.5	3.3	2	2.7	2.7	2.7	2.8	2.4	2.8
Pb	0.33	0.27	0.37	0.34	0.45	0.35	0.55	0.74	0.35	0.44
Th	0.1	<0.1	0.1	0.1	<0.1	0.2	0.2	1.2	1	0.9
U	0.05	0.04	0.05	0.06	0.04	0.07	0.08	0.34	0.17	0.16
La	2.5	2.1	3.4	3	3.6	2.9	3.4	8.8	6.9	8
Ce	8.1	6.6	12.2	9.2	12.1	9.9	10.2	20.3	16.3	19
Pr	1.4	1.13	2.2	1.54	2.1	1.85	1.78	2.9	2.45	2.81
Nd	7.7	6.3	12.9	8.4	11.8	10.4	10.3	13.7	12	13.4
Sm	2.8	2.3	4.5	3	4.3	4.1	3.8	3.9	3.4	3.9
Eu	1.08	0.84	1.62	1.07	1.55	1.3	1.35	1.53	1.16	1.42
Gd	3.6	3.1	6.2	3.8	5.6	5.4	5.4	4.6	4	4.8
Tb	0.7	0.6	1.2	0.7	1	1.1	1.1	0.9	0.7	0.9
Dy	4.5	3.8	7.7	4.6	6.8	7	6.9	5.2	4.6	5.4
Ho	0.9	0.8	1.6	1	1.4	1.5	1.4	1	0.9	1.1
Er	2.9	2.4	5	2.9	4.4	4.4	4.3	2.8	2.6	3
Tm	0.44	0.39	0.75	0.45	0.69	0.69	0.67	0.42	0.41	0.47
Yb	2.8	2.5	5	2.9	4.5	4.7	4.4	2.7	2.6	2.9
Lu	0.39	0.34	0.74	0.43	0.65	0.68	0.64	0.37	0.36	0.42
$(La/Yb)_N$	0.64	0.60	0.49	0.74	0.57	0.44	0.55	2.34	1.90	1.98

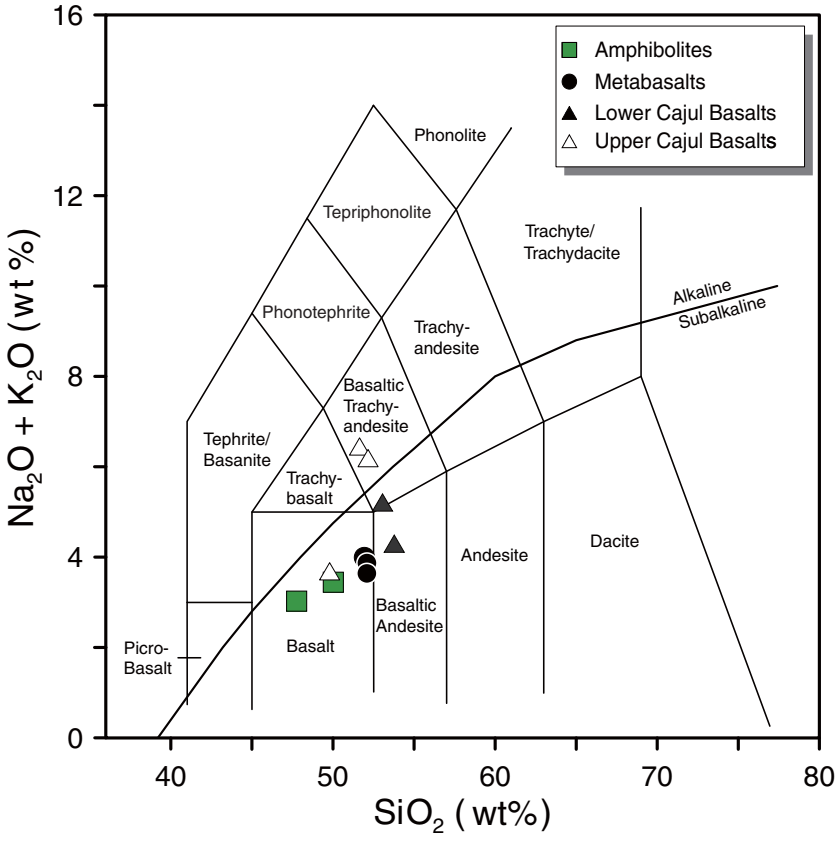

Figure 4. (Colour online) Classification of basaltic rocks in terms of SiO_2 v. total alkali (Le Maitre *et al.* 1989).

https://doi.org/10.1017/S001675681500093X Published online by Cambridge University Press

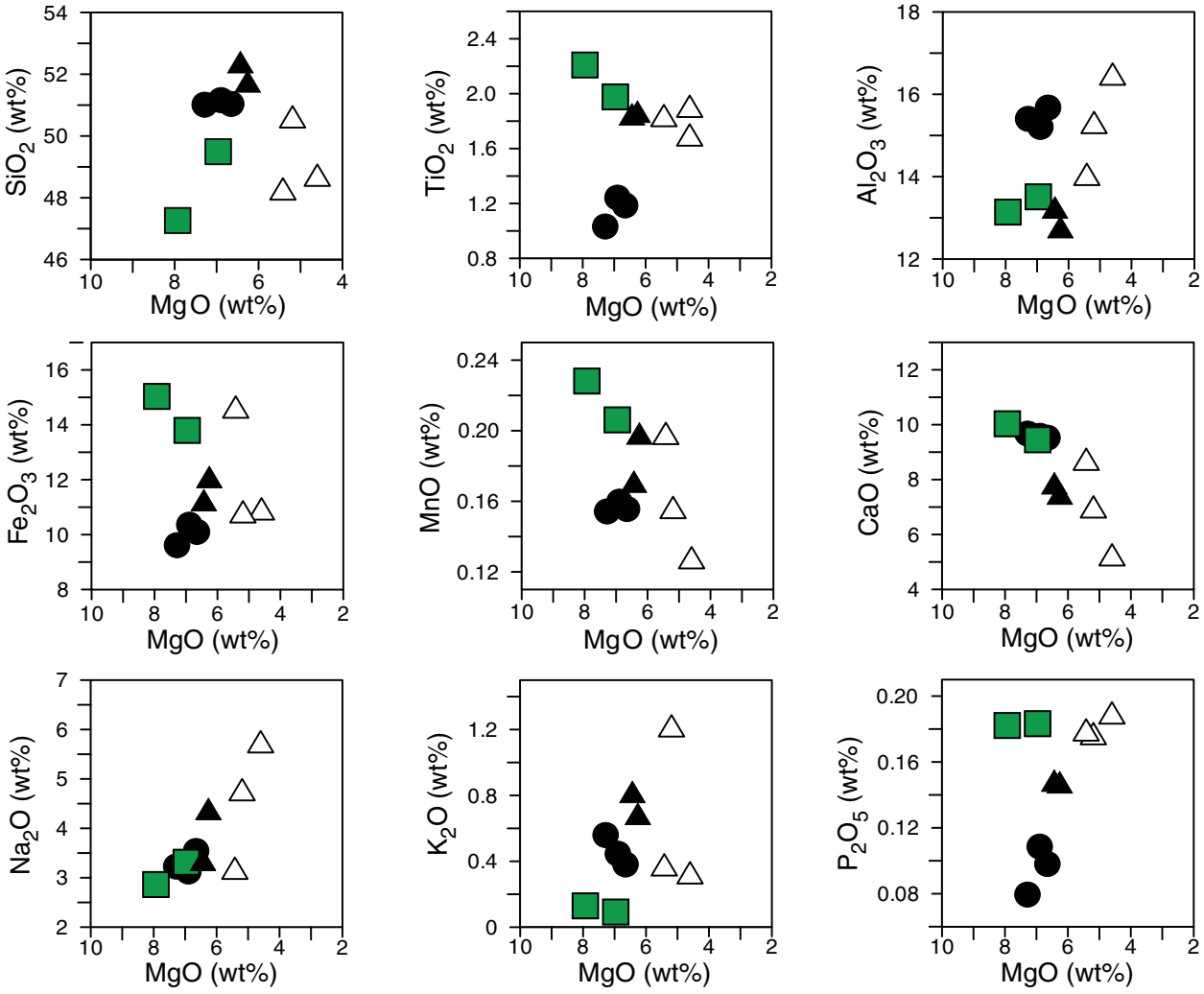

Figure 5. (Colour online) Major oxide variations for basaltic rocks from the Sierra Bermeja Complex. Symbols as in Figure 4.

exhibited a depleted N-MORB-like pattern. However, we observed weak enrichments in Cs, Ba and Rb, which are fluid mobile elements, and a depletion in Sr in the amphibolites compared to the N-MORB. Together with the negative Eu anomaly observed in the amphibolites, the negative Sr anomaly (Fig. 6a, c) reflects the effect of plagioclase fractionation. The metabasalts were more enriched in highly incompatible elements such as Cs, Rb, Ba and K compared to the amphibolites, and were characterized by negative Nb and positive Sr anomalies (Fig. 6c). The Lower Cajul basalts resembled the metabasalts, exhibiting enrichments in Cs, Rb, Ba and K and a weak negative anomaly in Nb (Fig. 6c). The Upper Cajul basalts generally resembled E-MORB, but sample PRNUC02 had positive anomalies in Cs, Rb, K and Sr and negative anomalies in U and Pb (Fig. 6d).

4.b.2. Isotopes

The Sr–Nd–Pb–Hf isotopic compositions are given in Table 3 and are illustrated in a series of isotopic correlation diagrams (Figs 7–9). For comparison, the fields for Atlantic and Pacific MORBs and for Caribbean Plateau basalts are also shown. Age corrections were applied after Jolly, Schellekens & Dickin (2007): 185 Ma for the amphibolites, metabasalts and Lower Cajul basalts, and 85 Ma for the Upper Cajul basalts.

The variation in the Sr–Nd–Hf–Pb isotopic compositions for the amphibolites was limited, with $(^{87}Sr/^{86}Sr)_i$ = 0.70361–0.70367; $(^{143}Nd/^{144}Nd)_i$ = 0.512829–0.512865 ($(\varepsilon_{Nd})_i$ = 8.4–9.1); $(^{176}Hf/^{177}Hf)_i$ = 0.283155–0.283219 ($(\varepsilon_{Hf})_i$ = 17.6–19.9); $(^{206}Pb/^{204}Pb)_i$ = 17.93–18.19; $(^{207}Pb/^{204}Pb)_i$ = 15.47–15.49; and $(^{208}Pb/^{204}Pb)_i$ = 37.61–37.74. The metabasalts exhibited more radiogenic Sr, Nd and Hf and less radiogenic Pb isotopic compositions: $(^{87}Sr/^{86}Sr)_i$ = 0.70339–0.70380; $(^{143}Nd/^{144}Nd)_i$ = 0.512879–0.512881 ($(\varepsilon_{Nd})_i$ = 9.3–9.4); $(^{176}Hf/^{177}Hf)_i$ = 0.283095–0.283100 ($(\varepsilon_{Hf})_i$ = 15.5–15.7); $(^{206}Pb/^{204}Pb)_i$ = 17.83–17.93; $(^{207}Pb/^{204}Pb)_i$ = 15.47–15.50; and $(^{208}Pb/^{204}Pb)_i$ = 37.47–37.61. The Lower Cajul basalts had a limited range of more radiogenic Sr–Pb and less radiogenic Nd–Hf isotopic compositions than the amphibolites: $(^{87}Sr/^{86}Sr)_i$ = 0.70384; $(^{143}Nd/^{144}Nd)_i$ = 0.512811–0.512819 ($(\varepsilon_{Nd})_i$ = 8.0–8.2); $(^{176}Hf/^{177}Hf)_i$ = 0.283044 ($(\varepsilon_{Hf})_i$ = 13.7); $(^{206}Pb/^{204}Pb)_i$ = 18.28–18.47; $(^{207}Pb/^{204}Pb)_i$ = 15.49; and $(^{208}Pb/^{204}Pb)_i$ = 37.77–37.87. The Upper Cajul

https://doi.org/10.1017/S001675681500093X Published online by Cambridge University Press

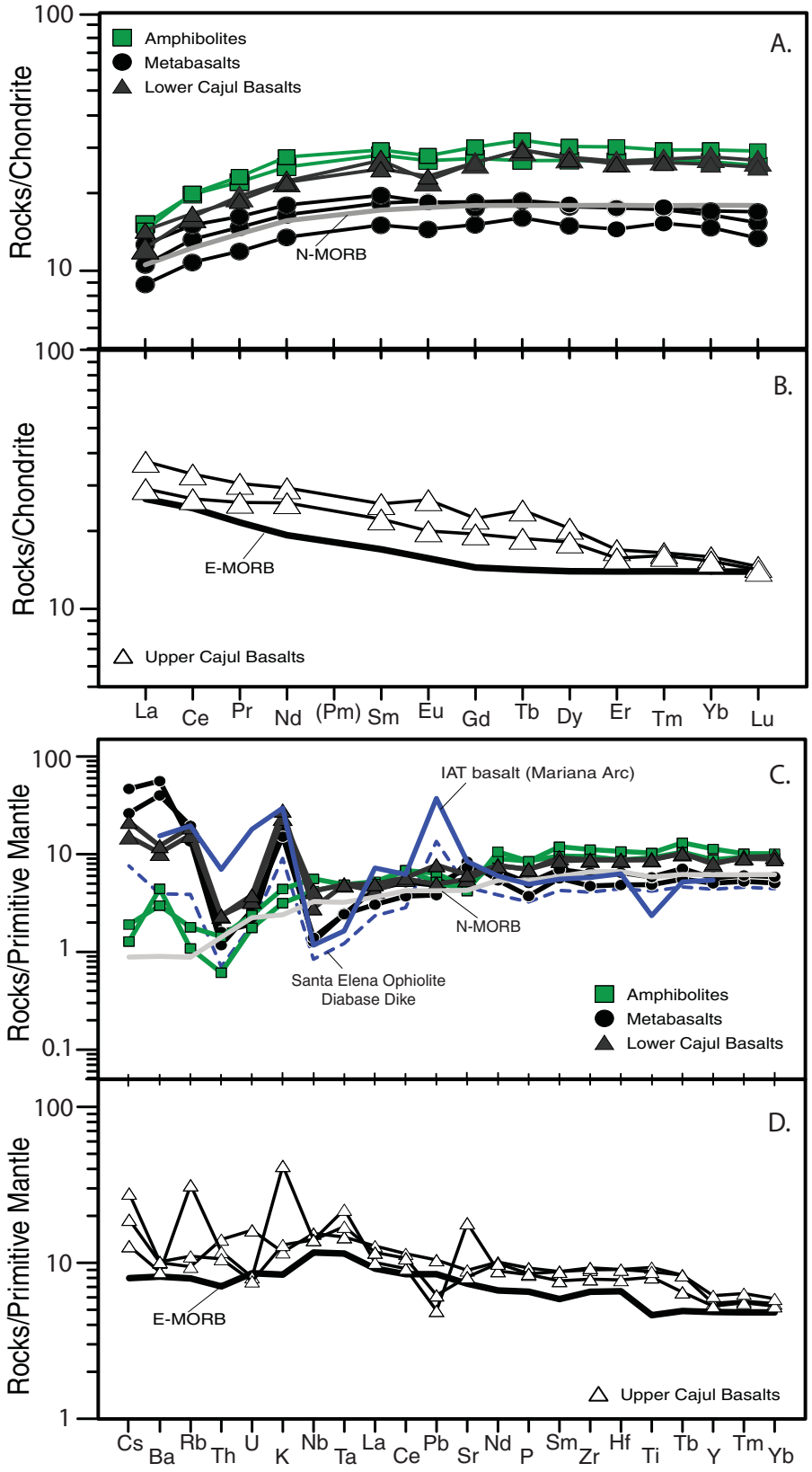

Figure 6. (Colour online) Chondrite-normalized rare earth element patterns for (a) amphibolites, metabasalts and Lower Cajul basalts, and (b) Upper Cajul basalts from the Sierra Bermeja Complex. Primitive mantle-normalized trace-element abundance patterns for (c) amphibolites, metabasalts and Lower Cajul basalts, and (d) Upper Cajul basalts. Normal mid-ocean-ridge basalt (N-MORB) and enriched mid-ocean ridge basalt (E-MORB) compositions are from Sun & McDonough (1989). Island-arc tholeiite (IAT) basalt from the Mariana arc (Gazel *et al.* 2011) and Santa Elena ophiolite diabase dyke (Madrigal *et al.* 2015) are also shown for comparison.

https://doi.org/10.1017/S001675681500093X Published online by Cambridge University Press

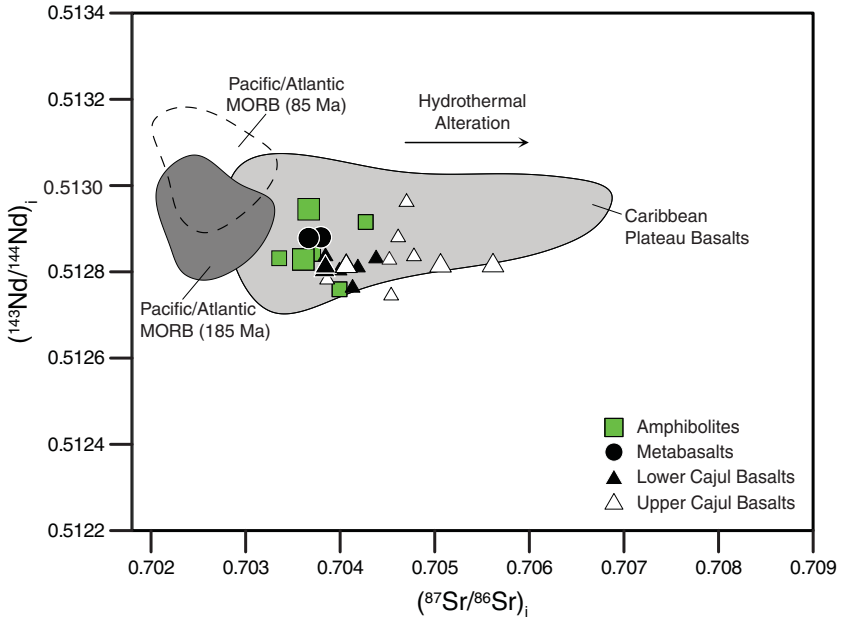

Figure 7. (Colour online) Age-corrected $^{143}Nd/^{144}Nd$ versus $^{87}Sr/^{86}Sr$ ratios for basaltic rocks from the Sierra Bermeja Complex. Data sources: Pacific/Atlantic MORB (Ito, White & Gopel, 1987; Bach *et al.* 1994; Mahoney *et al.* 1994; Niu *et al.* 1999; Chauvel & Blichert-Toft, 2001), Caribbean Plateau basalts (Hauff *et al.* 1999, 2000; White *et al.* 1999; Mamberti *et al.* 2003; Hastie *et al.* 2008). Errors (2σ) are within the size of the symbol in the plot.

basalts were characterized by a wide range of highly radiogenic Sr and Pb isotopic compositions: $(^{87}Sr/^{86}Sr)_i$ = 0.70406–0.70562; $(^{206}Pb/^{204}Pb)_i$ = 18.71–18.96; $(^{207}Pb/^{204}Pb)_i$ = 15.57–15.61; and $(^{208}Pb/^{204}Pb)_i$ = 38.37–38.62. Their Nd and Hf isotopic compositions were the least radiogenic among the samples studied: $(^{143}Nd/^{144}Nd)_i$ = 0.512821–0.512823 ($(\varepsilon_{Nd})_i$ = 5.7); and $(^{176}Hf/^{177}Hf)_i$ = 0.283011–0.283055 ($(\varepsilon_{Hf})_i$ = 11.9–12.5).

In the Sr–Nd isotope correlation diagram (Fig. 7), the amphibolites, metabasalt and Lower Cajul basalts are positioned slightly to the right of the Pacific/Atlantic MORB field. The Upper Cajul basalts have highly enriched Sr isotopic ratios compared to those of the amphibolites, metabasalts and Lower Cajul basalts, being widely spread with a subhorizontal trend. With regard to the isotopic composition of Pb for the basaltic samples, a large contrast exists between the older amphibolites, metabasalts and Lower Cajul basalts and the younger Upper Cajul basalts, with the latter having significantly higher Pb isotopic ratios than those for the amphibolites, metabasalts and Lower Cajul basalts. With the exception of the Lower Cajul Basalts, the samples are positioned above the Northern Hemisphere reference line (NHRL; Hart, 1984) in the Pb–Pb isotope correlation diagrams (Fig. 8). The amphibolite samples, together with metabasalts and the Lower Cajul basalts, are positioned within the age-corrected Pacific MORB field, whereas the younger Upper Cajul basalts are positioned outside the Pacific MORB field and fall more into the Caribbean Plateau basalts field. In the Nd–Hf isotope correlation diagram (Fig. 9), the amphibolites, metabasalt and Lower Cajul basalts are positioned within the age-corrected Pacific/Atlantic MORB field. The Upper Cajul basalts are positioned outside the MORB field, and fall within the range of Caribbean Plateau basalts (Fig. 9).

5. Discussion

5.a. *P–T* estimation

Two-pyroxene geothermometers (*T*/Wells (Wells, 1977) and *T*/BKN (Brey & Köhler, 1990)), calibrated for the solubility of the enstatite component in diopside coexisting with orthopyroxene, were used to estimate equilibration temperatures. The accuracy of the models was within ±70 °C. The results are presented in online supplementary Table S1 (available at http://journals.cambridge.org/geo). The peridotites from Monte del Estado had equilibrium temperatures of 870–970 °C for *T*/Wells and 800–960 °C for *T*/BKN. Peridotite from Rio Guanajibo exhibited an elevated temperature of 1040 °C with both geothermometers (Table S1). The two thermometers yielded consistent results within the observed level of accuracy (Fig. 10).

The Ca-in-olivine/clinopyroxene geobarometer of Köhler & Brey (1990) is a unique model that is used to estimate the pressure of spinel peridotites. The estimated temperature (*T*/BKN) was used as the input temperature for the pressure estimation. The results are presented in online supplementary Table S1 (available at http://journals.cambridge.org/geo). The estimated pressures were 26–72 kbar for peridotites from Monte del Estado and 92 kbar for Rio Guanijibo. Peridotites carrying spinel as a principal aluminous phase are considered stable at pressures of 8–25 kbar (Nickel, 1986; Webb & Wood, 1986). The estimated pressures

https://doi.org/10.1017/S001675681500093X Published online by Cambridge University Press

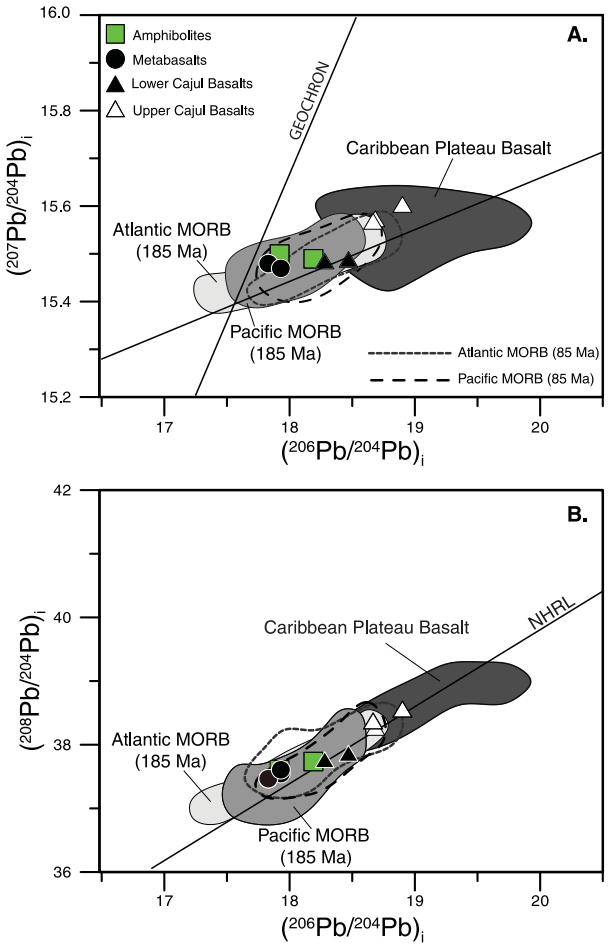

Figure 8. (Colour online) Age-corrected (a) $^{207}Pb/^{204}Pb$ v. $^{206}Pb/^{204}Pb$ and (b) $^{208}Pb/^{204}Pb$ v. $^{206}Pb/^{204}Pb$ ratios for basaltic rocks from the Sierra Bermeja Complex. Fields for the Pacific/Atlantic MORB and Caribbean Plateau basalts are shown for comparison. Data sources: Pacific/Atlantic MORB (Ito, White & Gopel, 1987; Mahoney *et al.* 1994; Niu *et al.* 1999; Kempton *et al.* 2000; Chauvel & Blichert-Toft, 2001; Debaille *et al.* 2006) and Caribbean Plateau basalts (Hauff *et al.* 1999, 2000; White *et al.* 1999; Mamberti *et al.* 2003; Thompson *et al.* 2003; Hastie *et al.* 2008). The Northern Hemisphere reference line (NHRL) is from Hart (1984). Errors (2σ) are within the size of the symbol in the plot.

therefore exceeded the upper limit of the spinel stability field. The Ca-in-olivine/clinopyroxene geobarometer is highly temperature-dependent and sensitive to the diffusion of Ca in olivine (Köhler & Brey, 1990). The diffusion coefficient of Ca in olivine is 3–4 orders of magnitude higher than that in clinopyroxene (Köhler & Brey, 1990). These unrealistically high pressures might have been induced by intense cooling with re-equilibration of olivines to low temperatures during shallow-level intrusions of the peridotite bodies. The peridotites moved upwards, possibly along shallow-angle thrust faults (Laó-Dávila, Llernadi-Román & Anderson, 2012).

5.b. Petrogenesis of peridotites

Spinel Cr no. is a sensitive indicator of the extent to which the spinel peridotites have lost basaltic components (e.g. Dick & Bullen, 1984; Aswad, Aziz & Koyi, 2011). The Fo olivine content can also provide information regarding the degree of melt depletion in mantle peridotites (Arai, 1994). Spinel Cr no. and Mg no., as well as the olivine Fo composition, were used to identify the tectonic setting of the formation of the Puerto Rico peridotites (Fig. 2a, b). The spinel Cr no. of abyssal peridotites ranged over *c.* 10–55. Suprasubduction zone peridotites are characterized by spinels with much higher Cr numbers than abyssal peridotites, ranging over *c.* 38 to >80 (Fig. 2a, b). With the increasing degree of melt depletion, the spinel Cr no. grew with the increase of olivine Fo content within the olivine–spinel mantle array (Fig. 2b). On a diagram of spinel Cr no. versus spinel Mg no. (Fig. 2a), the Puerto Rico peridotites are positioned inside the abyssal peridotite field. They also belong to the abyssal peridotites in terms of the Fo of olivine and Cr no. of spinel (Fig. 2b). However, it should be noted that the spinels from the Sierra Bermeja Complex peridotites had a higher Cr no. than those from the Monte del Estado and Rio Guanajibo peridotites. The TiO_2 content in the spinel from the Monte del Estado and Rio Guanajibo peridotites was low (≤0.07 wt %) and incompatible with the Sierra Bermeja samples, in which the TiO_2 content reached 0.10 wt % (online supplementary Table S1, available at http://journals.cambridge.org/geo). When spinel Cr

https://doi.org/10.1017/S001675681500093X Published online by Cambridge University Press

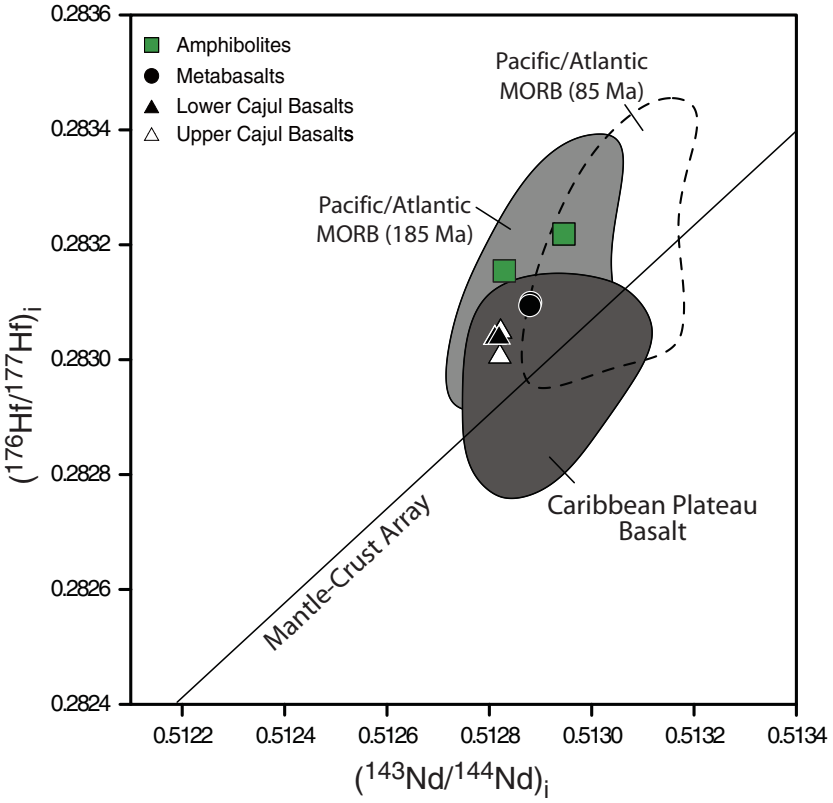

Figure 9. (Colour online) Age-corrected $^{176}Hf/^{177}Hf$ v. $^{143}Nd/^{144}Nd$ ratios for basaltic rocks from the Sierra Bermeja Complex. Fields for the Pacific/Atlantic MORB and Caribbean Plateau basalts are shown for comparison. Data sources: Pacific/Atlantic MORB (Ito, White & Gopel, 1987; Mahoney *et al.* 1994; Nowell *et al.* 1998; Salters & White, 1998; Niu *et al.* 1999; Chauvel & Blichert-Toft, 2001) and Caribbean Plateau basalts (Hauff *et al.* 1999, 2000; White *et al.* 1999; Geldmacher *et al.* 2003; Mamberti *et al.* 2003; Thompson *et al.* 2003; Hastie *et al.* 2008). The mantle–crust array is from Blichert-Toft & Albarède (1997). Errors (2σ) are within the size of the symbol in the plot.

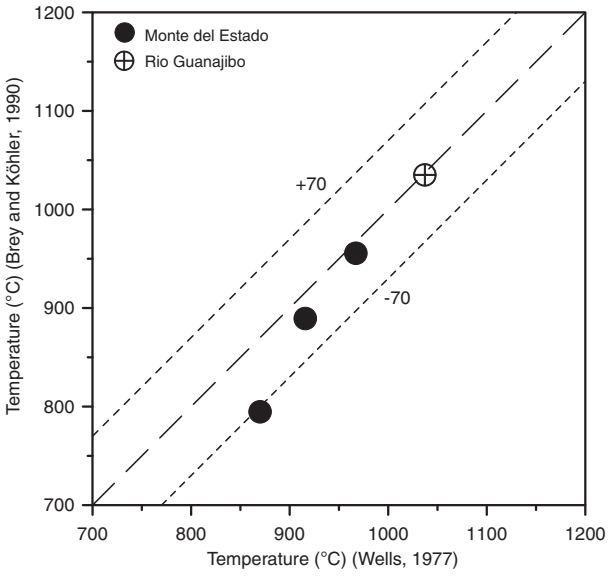

Figure 10. Comparison of temperature estimates from the two-pyroxene thermometers of Brey & Köhler (1990) and Wells (1977) for peridotites from Monte del Estado and Rio Guanajibo.

no. was plotted against spinel TiO_2 content (Fig. 11), it was apparent that the Monte del Estado and Rio Guanajibo peridotites were positioned within the most fertile abyssal peridotite field, close to the modelled depletion trend from the fertile MORB mantle (FMM). However, the peridotite spinels from the Sierra Bermeja Complex departed from the modelled trend, with higher TiO_2 content similar to that of abyssal peridotites that reacted with a MORB-like melt.

Hellebrand *et al.* (2001) developed a quantitative melting indicator for mantle residue as a function of spinel Cr no., yielding the relationship $F = 10 \ln(\text{Cr no.}) + 24$, where F (%) is the degree of partial melting. For the Sierra Bermeja and Rio Guanajibo samples, we obtained values for the degree of melting of 4–8 %, whereas for the Sierra Bermeja Complex peridotites the range was 8–14 % (almost twice the value of the Monte del Estado and Rio Guanajibo peridotites; Table S1). Oceanic crustal thickness can be calculated from the peridotite spinel compositions after Hellebrand, Snow & Mühe, (2002): $H = Z_0 F - (F^2/2B)$, where H is crustal thickness (km), $Z_0 = 70$ km, F is the degree of partial melting (%) and B is the melt production rate (km^{-1}). The crustal thickness above the Monte del Estado and Rio Guanajibo peridotites ranged over 2.3–4.8 km (Table S1), and above the Sierra Bermeja peridotites 4.8–6.9 km (Table S1). Given that the degree of melting and crustal thickness are directly related to the velocity at which a mid-ocean ridge spreads (Reid & Jackson, 1981), we assumed that the thinner block containing the Monte del Estado and

https://doi.org/10.1017/S001675681500093X Published online by Cambridge University Press

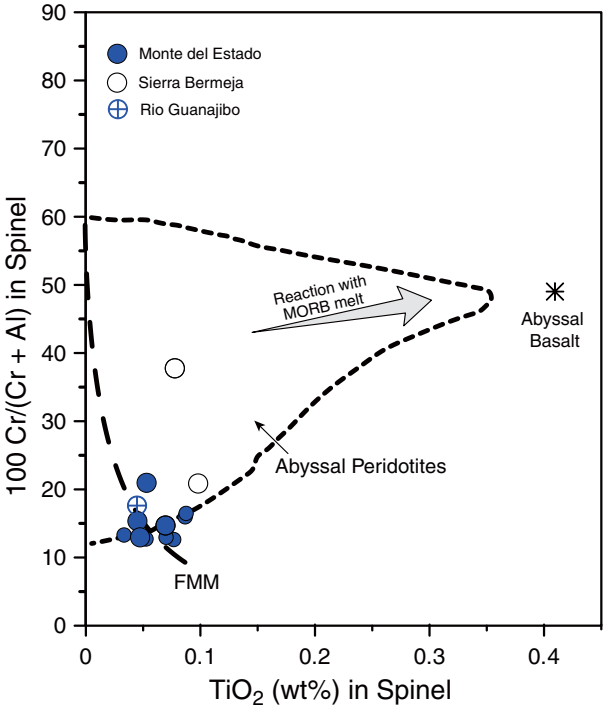

Figure 11. (Colour online) TiO_2 content v. 100 Cr/(Cr + Al) in the spinel of Puerto Rico peridotites. The line with short dashes represents the field of abyssal peridotite spinels. The grey arrow represents the effect of a MORB-like melt reaction on refractory abyssal peridotite spinels. The data for spinels from abyssal peridotites and basalt are from Dick & Bullen (1984).

Rio Guanajibo peridotites belonged to an ultra-slow-spreading ridge, whereas the block containing the Sierra Bermeja Peridotites belonged to a faster-spreading ridge.

To better constrain the petrogenesis and tectonic environment of the formation of the Puerto Rico peridotites, spinel Cr no. was plotted against the temperature obtained by the two-pyroxene geothermometer of Wells (1977) (Fig. 12). The fields for abyssal peridotites are shown for comparison, as well as the published data for other Caribbean abyssal peridotites. Large-offset transform fault-related peridotites are characterized by relatively lower equilibration temperatures than those of the small-offset or non-transform-setting abyssal peridotites (Fig. 12). In contrast to other Caribbean samples, the Monte del Estado peridotites are positioned outside the small-offset or non-transform-setting abyssal peridotite field. They fall within the fields for large-offset transform fault-related peridotites, such as the Vema Fracture Zone, Owen Fracture Zone and Romanche Fracture Zone (Fig. 12). The single available Rio Guanajibo peridotite is positioned along the boundary between the two settings. Large-offset transform fault-related peridotites were generally less depleted than the nearby centre segment peridotites, possibly due to the relatively lower degree of melting induced by the colder thermal regime (Choi, Mukasa & Shervais, 2008). Given the unrealistically high pressures estimated by the Ca-in-olivine/clinopyroxene geobarometer (online supplementary Table S1, available at http://journals.cambridge.org/geo) and the small degree of melting experienced by the Monte del Estado and Rio Guanajibo peridotites, we suggest that a large-offset transform fault might have induced intensive cooling in the peridotites.

5.c. Petrogenesis of basaltic rocks

The Las Palmas amphibolites had depleted N-MORB-like REE (Fig. 6a) and incompatible trace-element patterns (Fig. 6c). In the Pb–Pb (Fig. 8) and Nd–Hf (Fig. 9) isotopic correlation diagrams they are positioned within the range of Pacific/Atlantic MORB of similar age, reflecting their N-MORB origin. However, in the Sr–Nd isotopic plot (Fig. 7), the amphibolites are slightly to the right of the MORB field. Note also that they are slightly enriched in highly incompatible Cs, Ba and Rb when compared to the N-MORB in Figure 6c. During low-temperature alteration, Cs, Ba and Rb are highly mobile elements (Dostal, Dupuy & Pudoignon, 1996), and in hydrothermal fluids, Sr is a relatively mobile element (Kogiso, Tatsumi & Nakano, 1997). To better constrain the tectonic setting of the basaltic rocks, we compared their Ti–Zr–Y concentrations using Ti–Zr–Y (Fig. 13a), Zr/Y v. Zr (Fig. 13b) and Th/Yb v. Nb/Yb (Fig. 13c) discrimination diagrams. The use of these elements in petrogenetic modelling is practical because the high-field-strength elements are generally resistant to post-magmatic alteration or low-grade metamorphism (Pearce & Norry, 1979). The amphibolites fall within the MORB field on the Ti–Zr–Y and Zr/Y–Zr plots. They also have normal MORB-like Nb/Yb and Th/Yb ratios (Fig. 13c). Seawater had relatively high Sr concentrations (8 ppm) and high $^{87}Sr/^{86}Sr$ values of 0.7075 during Early Jurassic time (Veizer, 1989). The elevated $^{87}Sr/^{86}Sr$ ratios of the amphibolites could therefore be the result of submarine hydrothermal metamorphism.

The metabasalts and Lower Cajul basalts also had N-MORB-like LREE-depleted patterns (Fig. 6a). However, in contrast to the amphibolites, the primitive mantle-normalized incompatible trace-element patterns (Fig. 6c) indicate significant enrichment in highly incompatible elements (such as Cs, Ba, Rb and K), characteristic of a mantle wedge metasomatized by fluids from a subducting slab (Parlak *et al.* 2004). The slight depletion in Nb and enrichment in Sr should also be noted. In this respect, they resemble the island-arc tholeiite from the Mariana arc (Fig. 6c) and the diabase intrusion (*c.* 121 Ma) in the Santa Elena ophiolite, Costa Rica (Fig. 6c) formed in a slow/ultraslow-spreading back-arc basin (Madrigal et al. 2015). On the plots of Ti–Zr–Y (Fig. 13a) and Zr/Y v. Y (Fig. 13b), they are positioned along the boundary between the island-arc tholeiite and MORB fields, again marking their island-arc or back-arc affinity. Also note that they have Nb/Yb ratios less than normal MORB, and slightly elevated Th/Yb ratios plotting towards the

https://doi.org/10.1017/S001675681500093X Published online by Cambridge University Press

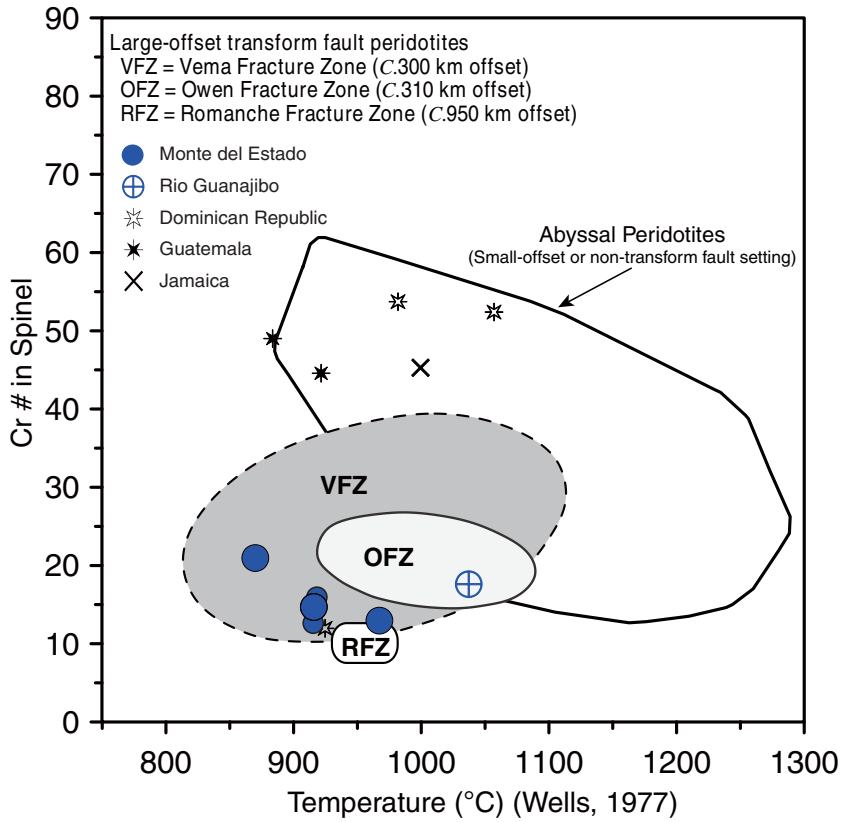

Figure 12. (Colour online) Cr no. (100 Cr/(Cr + Al)) in spinels from the Monte del Estado and Rio Guanajibo peridotites v. the equilibration temperatures estimated by the two-pyroxene thermometer of Wells (1977). The data for large-offset transform fault peridotites are from OFZ (Hamlyn & Bonatti, 1980), RFZ (Bonatti, Seyler & Sushevskaya, 1993), and VFZ (Brunelli *et al.* 2006). Data for small-offset or non-transform-setting abyssal peridotites from Choi *et al.* (2008). Data for peridotites from the Dominican Republic, Guatemala and Jamaica (Bourgois *et al.* 1984; Abbott, Jackson & Scott, 1999; Escuder-Viruete, Castillo-Carrion & Perez-Estaun, 2014) are also plotted for comparison.

subduction interaction vector in Figure 13c. In the Pb–Pb (Fig. 8) and Nd–Hf (Fig. 9) isotopic correlation diagrams, they are positioned within the range of Pacific/Atlantic MORBs of similar age. In the Sr–Nd isotope plot (Fig. 7) however, the $^{87}Sr/^{86}Sr$ ratios are elevated compared to the MORB at a given $^{143}Nd/^{144}Nd$. The elevated $^{87}Sr/^{86}Sr$ ratios could be the result of contamination by fluids dehydrated from a seawater-altered subducting slab.

The Upper Cajul basalts had E-MORB-like LREE and large-ion-lithophile element (LILE, e.g. K, Rb, Cs and Ba) enrichment (Fig. 6b, d). However, some samples exhibited positive anomalies in Cs, Rb, K and Sr and a negative anomaly in Pb (Fig. 6d). The slight enrichment in Nb and Ta (Fig. 6d) provides evidence that they were not generated in an island-arc or back-arc setting. Anomalously high Cs, Rb and K contents in the Upper Cajul basalts may be the product of low-temperature subaerial or submarine alteration, likely due to the mobility of these elements during surface processes (e.g. Dostal, Dupuy & Pudoignon, 1996). During submarine alteration, Sr can be mobile but Pb redistribution during low-temperature alteration is relatively small (Dostal, Dupuy & Pudoignon, 1996). Both Pb and Sr are highly mobile in hydrous fluids (Kogiso, Tatsumi & Nakano, 1997). The anomalous low Pb and high Sr that were observed in the Upper Cajul basalts might therefore have been produced by hydrothermal activity.

On the plots of Ti–Zr–Y (Fig. 13a) and Zr/Y v. Y (Fig. 13b), the Upper Cajul basalts are positioned along the boundary lines of MORB and within-plate basalt fields, being somehow ambiguous; they do plot along the E-MORB position on the Th/Yb v. Nb/Yb correlation (Fig. 13c) however, consistent with their E-MORB origin. The $^{87}Sr/^{86}Sr$ and $^{143}Nd/^{144}Nd$ isotopic compositions of the Upper Cajul basalts are however positioned outside the range of Pacific/Atlantic MORB of similar age (Fig. 7), precluding their derivation from the convective MORB source. For comparison, the available isotopic data for Caribbean oceanic plateau basalts are shown in the plot (Fig. 7). The Caribbean Plateau magmatism occurred during 95–72 Ma, with a peak at *c.* 92–88 Ma (Sinton *et al.* 1998; Hauff *et al.* 2000; Hastie *et al.* 2008). The Caribbean oceanic plateau basalts have E-MORB-like to transitional tholeiite basalt compositions, generated from a mantle plume and possibly recycled oceanic crust (Walker *et al.* 1999; Hauff *et al.* 2000). The Sr and Nd isotopic compositions of the Upper Cajul basalts are positioned along

https://doi.org/10.1017/S001675681500093X Published online by Cambridge University Press

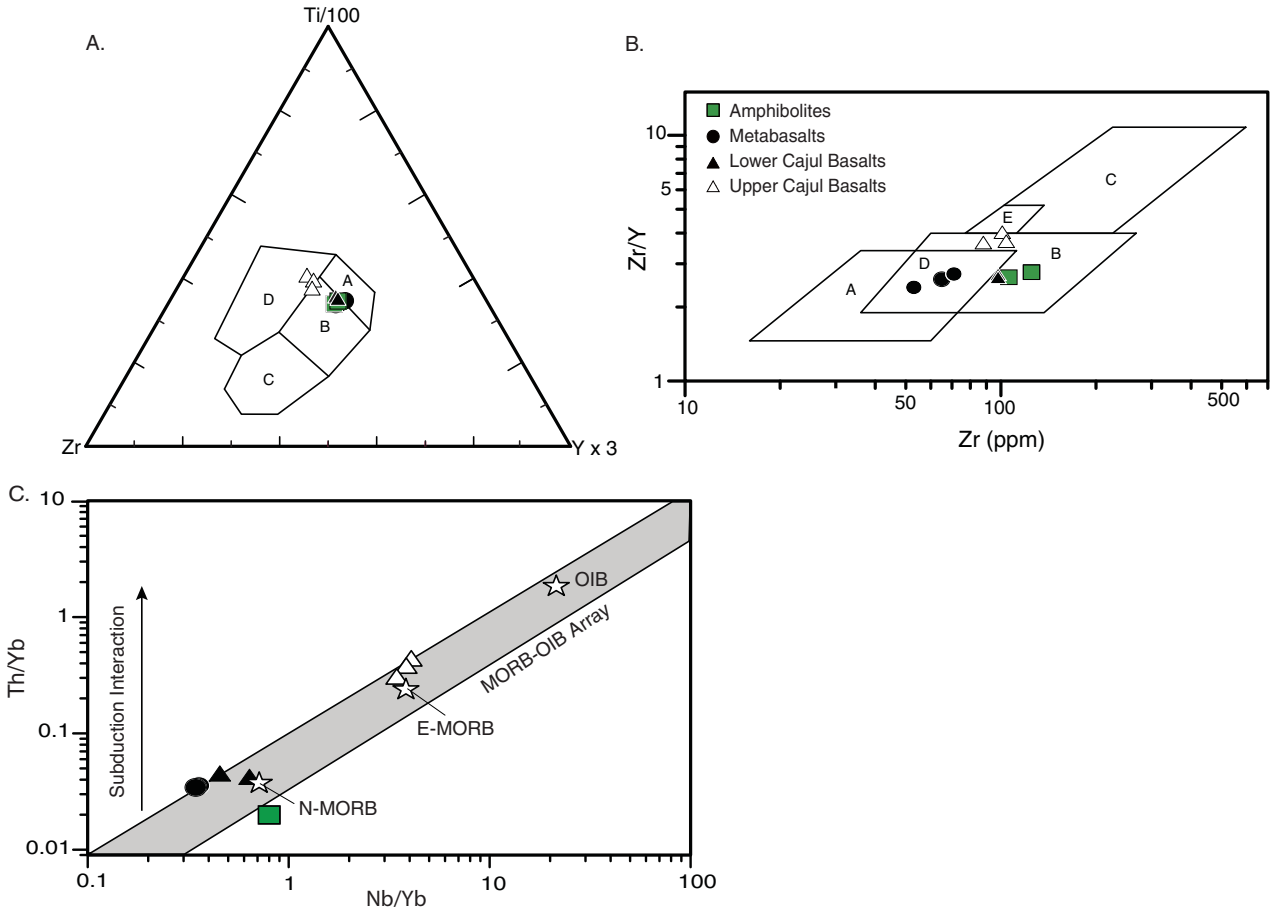

Figure 13. (Colour online) (a) Ti–Zr–Y tectonic discrimination diagram for basaltic rocks from the Sierra Bermeja Complex (after Pearce & Cann, 1973). A: field of island-arc tholeiites; B: field of mid-ocean-ridge basalt (MORB), island-arc tholeiites and calc-alkali basalts; C: field of calc-alkali basalts; D: field of within-plate basalts. (b) The Zr/Y v. Zr (ppm) tectonic diagram (after Pearce & Norry, 1979). A: field of volcanic-arc basalts; B: field of MORB; C: field of within-plate basalts: D: field of MORB and volcanic-arc basalts; E: field of enriched-MORB and within-plate basalts. (c) The Th/Yb v. Nb/Yb diagram (after Pearce & Peate, 1995). E-MORB – enriched MORB; OIB – oceanic-island basalt.

the enriched edge of the Caribbean Plateau basalt field (Fig. 7). The highly elevated $^{87}Sr/^{86}Sr$ ratios are a common feature of most Caribbean Plateau lavas, which are considered to have resulted from post-magmatic processes such as hydrothermal alteration rather than reflecting primary magmatic characteristics (Sinton *et al.* 1998; Thompson *et al.* 2003; Hastie *et al.* 2008). The $^{87}Sr/^{86}Sr$ increase in the Upper Cajul basalts might be due to secondary alteration. In the Pb–Pb isotopic correlation diagrams (Fig. 8), two samples (PRNUC02 and 03) are positioned within the range of Pacific/Atlantic MORB of similar age. However, one sample (PRNUC01) is positioned outside the range, falling within the field of the more radiogenic Caribbean Plateau basalts. Substantial alteration by seawater would not significantly alter the Pb isotope ratios because of the low abundance of Pb (2×10^{-6} ppm), Th (1×10^{-5} ppm) and U (3.2×10^{-3} ppm) in seawater (Brown *et al.* 1997, p. 86–87). The Pb isotopic values therefore probably represent the primary magmatic compositions of the Upper Cajul basalts. The Nd and Hf isotope systems are more resistant to alteration or metamorphism than the Sr and Pb isotopic system; their ratios therefore represent the primary compositions of the lavas (e.g. White & Patchett, 1984). In the Nd–Hf isotopic correlation diagram (Fig. 9), the Upper Cajul basalts falls within the range of the Caribbean oceanic plateau basalts. We therefore conclude that the Upper Cajul basalts are likely the tectonized equivalent of the Caribbean oceanic plateau.

5.d. Tectonic implications

Palaeomagnetic data indicate that a thin proto-Caribbean ocean floor (less than 5 km in thickness) began to form between the North and South American plates during Jurassic and Early Cretaceous time (153–127 Ma) at an ultra-slow spreading rate of 0.4–0.5 cm a^{-1} (Ghosh, Hall & Casey, 1984). Based on a palaeotectonic reconstruction of the Cretaceous Caribbean realm, Marchesi *et al.* (2011) proposed that the Monte del Estado peridotite belt might be the ancient Proto-Caribbean lithospheric mantle. Our results showing the relatively fertile mineral compositions, low degree of melting and low equilibration temperatures suggest that the Monte del

https://doi.org/10.1017/S001675681500093X Published online by Cambridge University Press

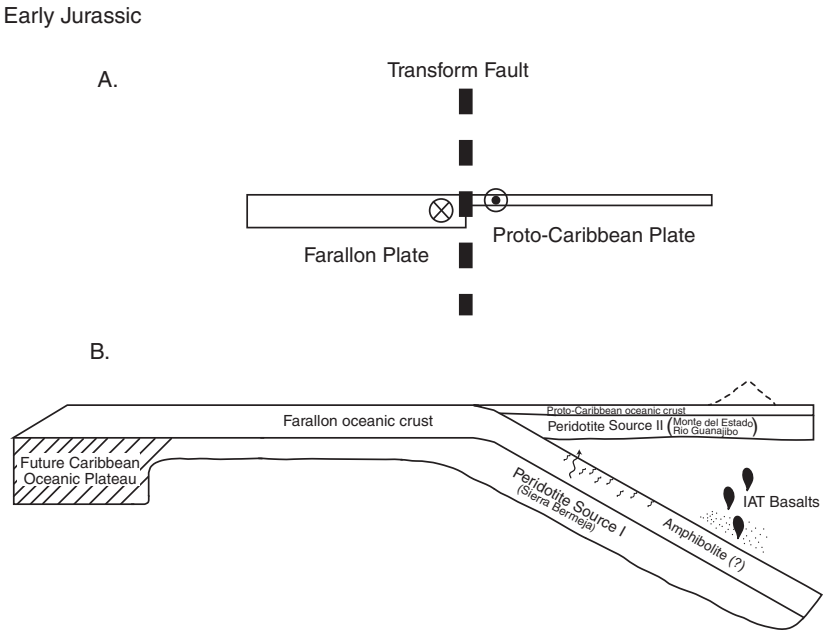

Figure 14. Cross-section of suggested local plate evolution represented in the SW Igneous Province of Puerto Rico. (a) Eventual transform fault relation between the Farallon and Proto-Caribbean plates and (b) subduction initiation of the Farallon Plate under the Proto-Caribbean Plate during Early Jurassic time. Peridotite Source I for the Sierra Bermeja peridotites; Peridotite Source II for the Monte del Estado and Rio Guanajibo peridotites; IAT – island-arc tholeiite.

Estado and Rio Guanajibo peridotites might be the slow-spreading proto-Caribbean large-offset transform fault-related oceanic lithospheric mantle. With their relatively high spinel Cr no., the Sierra Bermeja peridotites are likely to have been the comparatively fast-spreading proto-Pacific (Farallon) lithospheric mantle.

Schellekens (1998*a*) suggested that the Sierra Bermeja amphibolites might be the remnants of a transform fault at the ocean floor that initiated subduction in this area, and could be the same large-offset transform fault that is believed to have imposed a cold thermal regime on the lithospheric mantle beneath the Monte del Estado. The amphibolites may represent the subducted fragments of the Farallon oceanic plate basalts or metamorphic soles formed in a hanging wall (Wakabayashi & Dilek, 2003). The metamorphic age of the amphibolites (126±3 Ma; Cox *et al.* 1977) indicates that they underwent metamorphism during Early Cretaceous time. A new subduction zone can form along pre-existing lithospheric weakness zones, such as transform faults (e.g. Casey & Dewey, 1984; Stern & Bloomer, 1992). We suggest that the eastwards subduction might have been initiated along a large-offset transform fault, and the Monte del Estado peridotite could be part of the intact Proto-Caribbean lithospheric mantle trapped in the forearc of an eastwards-subducting slab (Fig. 14). The Sierra Bermeja peridotites were likely emplaced into a serpentinite subduction channel by tectonic off-scraping from the down-going Farallon Plate (Fig. 14). The island-arc tholeiite basalt-like Sierra Bermeja metabasalts and Lower Cajul basalt were produced in the suprasubduction zone by the eastwards subduction of the Farallon Plate (Fig. 14). A subduction complex can be active for many tens of millions of years (e.g. Brueckner *et al.* 2009). Determining the exact timing of the subduction initiation and duration will be the focus of future work.

The Caribbean Plate is moving eastwards relative to North and South America at a rate of *c.* 2 cm a^{-1}, although the exact velocity is controversial (e.g. Jansma *et al.* 2000). Plate reconstructions of the tectonic evolution of the Caribbean Plate generally propose that the plateau formed *c.* 90 Ma in the eastern Pacific region as part of the Farallon (proto-Pacific) Plate, in the vicinity of the present-day Galápagos hotspot, and this was followed by a NE-directed motion (Burke, Fox & Şengőr, 1978; Duncan & Hargraves, 1984; Herzberg & Gazel, 2009; Gazel, Abbott & Draper, 2011). Shortly after its formation the plateau collided with the Greater Antilles Arc, which extended along the Pacific margin of the proto-Caribbean. This resulted in a reversal in the polarity of subduction from east to west, possibly due to its buoyancy, and the subsequent emplacement of the plateau between North and South America (Burke, 1988; Pindell & Barrett, 1990, p. 426; Kerr & Tarney, 2005). Fossil evidence from the Greater Antilles also suggests a Pacific origin for the plateau. Chert intercalated with the Cajul basalts contains Early Jurassic and mid-Cretaceous radiolarians derived from the subducting Farallon Plate (Montgomery, Pessagno & Pindell, 1994; Bandini *et al.* 2011). Recently, Pindell *et al.* (2012) and Boschman *et al.* (2014) suggested that the Greater Antillean Arc formed at around or before 135 Ma by inception of SW-dipping subduction along an 'inter-American transform' connecting the west-facing subduction zones of the North and South American Cordillera, without an arc polarity reversal.

https://doi.org/10.1017/S001675681500093X Published online by Cambridge University Press

We note however that this model is hard to reconcile with the fossil evidence together with the NE-dipping subduction polarity based on distribution of Late Cretaceous high-Mg andesites and related lavas from the SIP of Puerto Rico (Jolly, Schellekens & Dickin, 2007). We suggest that the Upper Cajul basalts belong to the tectonized Caribbean oceanic plateau basalts, as it has also been suggested by Lidiak, Jolly & Dickin (2011). This observation, together with the overlying Campanian limestone and intrusive Maguayo Porphyry (86 Ma), indicates that the serpentinites must have been emplaced during Coniacian–Turonian time (Laó-Dávila, 2014).

6. Conclusions

1. Peridotite bodies found in the SW block of Puerto Rico originated in two different tectonic settings. The Monte del Estado and Rio Guanajibo peridotites, with low spinel Cr no., might be the ultra-slow-spreading proto-Caribbean oceanic lithospheric mantle. The Sierra Bermeja peridotites, with higher Cr no. and TiO_2 content, likely originated from the relatively fast-spreading Farallon Plate lithospheric mantle.

2. The two lithospheric mantles are related to each other by a large-offset transform fault, which caused intensive cooling. The proto-Caribbean mantle peridotites were trapped in the forearc of the eastwards-subducting Farallon Plate, while tectonic off-scraping from the down-going proto-Pacific lithospheric mantle emplaced the Sierra Bermeja peridotites into the subduction channel.

3. REE and trace-element patterns and Sr–Nd–Hf–Pb isotopic compositions indicate an ancient Pacific N-MORB origin for the Sierra Bermeja amphibolites and an island-arc tholeiitic melt origin for the Lower Cajul basalts and metabasalts, which were affected by fluids dehydrated from a seawater-altered subducting slab. We suggest that the formation of the metabasalts and Lower Cajul basalts could be related to the subduction initiated by the large-offset transform fault and that they formed in a mantle wedge as the Pacific N-MORB-type amphibolite protoliths were subducted.

4. E-MORB-like Upper Cajul basalts are considered to be tectonized equivalents of the Caribbean oceanic plateau basalts. Highly elevated $^{87}Sr/^{86}Sr$ isotopic ratios indicate post-magmatic hydrothermal alteration, which is a characteristic of Caribbean plateau-related basalts. The Pb–Pb and Nd–Hf isotopic correlations indicate primary Caribbean plateau basalt composition.

Acknowledgements. This research was supported by the Basic Science Research Program through the National Research Foundation of Korea (NRF) funded by the Ministry of Science, ICT and Future Planning (NRF-2013R1A2A2A01004382 and NRF-2013R1A2A1A01004418). We would like to thank James Joyce, Fernando Martínez Torres, Nak Kyu Kim and Francisco Hernández for their assistance with fieldwork. Insightful reviews by Esteban Gazel and an anonymous reviewer greatly improved the manuscript.

References

ABBOTT, R. N., JACKSON, T. A. & SCOTT, P. W. 1999. The serpentinization of peridotite from Cedar Valley, Jamaica. *International Geology Review* **41**, 836–44.

ARAI, S. 1994. Characterization of spinel peridotites by olivine–spinel compositional relationships: review and interpretation. *Chemical Geology* **113**, 191–204.

ASWAD, K. J. A., AZIZ, N. R. H. & KOYI, H. A. 2011. Cr-spinel compositions in serpentinites and their implications for the petrogenetic history of the Zagros Suture Zone, Kurdistan Region, Iraq. *Geological Magazine* **148**, 802–18.

BACH, W., HEGNER, E., ERZINGER, J. & SATIR, M. 1994. Chemical and isotopic variations along the superfast spreading East Pacific Rise from 6 to 30° S. *Contributions to Mineralogy and Petrology* **116**, 365–80.

BANDINI, A. N., BAUMGARTNER, P. O., FLORES, K., DUMITRICA, P., HOCHARD, C., STAMPFLI, G. M. & JACKETT, S. J. 2011. Aalenian to Cenomanian Radiolaria of the Bermeja complex (Puerto Rico) and Pacific origin of radiolarites on the Caribbean plate. *Swiss Journal of Geoscience* **104**, 367–408.

BEDINI, R. M. & BODINIER, J.-L. 1999. Distribution of incompatible trace elements between the constituent of spinel peridotite xenoliths: ICP-MS data from the East African Rift. *Geochimica et Cosmochimica Acta* **63**, 3883–900.

BLICHERT-TOFT, J. & ALBARÈDE, F. 1997. The Lu–Hf isotope geochemistry of chondrites and the evolution of the mantle–crust system. *Earth and Planetary Science Letters* **148**, 243–58.

BODINIER, J.-L. & GODARD, M. 2003. Orogenic, ophiolitic, and abyssal peridotites. In *The Mantle and Core* (eds R. W. Carlson, H. D. Holland & K. K. Turekian), pp. 103–70. Elsevier-Pergamum, Treatise on Geochemistry Vol. 2.

BONATTI, E., SEYLER, M. & SUSHEVSKAYA, N. 1993. A cold suboceanic mantle belt at the Earth's equator. *Science* **261**, 315–20.

BOSCHMAN, L. M., VAN HINSBERGEN, D. J. J., TORSVIK, T. H., SPAKMAN, W. & PINDELL, J. L. 2014. Kinematic reconstruction of the Caribbean region since the Early Jurassic. *Earth-Science Reviews* **138**, 102–36.

BOURGOIS, J., DESMET, A., TOURNON, J. & AUBOUIN, J. 1984. Mafic and ultramafic rocks of LEG 84: Petrology and Mineralogy. *Ophioliti* **9**, 27–42.

BREY, G. P. & KÖHLER, T. P. 1990. Geothermobarometry in four-phase lherzolites II. New thermobarometers, and practical assessment of existing thermobarometers. *Journal of Petrology* **31**, 1353–78.

BROWN, E., COLLING, A., PARK, D., PHILLIPS, J., ROTHERY, D. & WRIGHT, J. 1997. *Seawater: Its Composition, Properties and Behavior*. Milton Keynes: Open University, Open University Course Team, pp. 86–87.

BRUECKNER, H. H., AVÉ LALLEMANT, H. G., SISSON, V. B., HARLOW, G. E., HEMMING, S. R., MARTENS, U., TSUJIMORI, T. & SORENSEN, S. S. 2009. Metamorphic reworking of a high pressure-low temperature mélange along the Motagua fault, Guatemala: a record of Neocomian and Maastrichtian transpressional tectonics. *Earth and Planetary Science Letters* **284**, 228–35.

BRUNELLI, D., SYLER, M., CIPRIANTI, A., OTTOLINI, L. & BONATTI, E. 2006. Discontinuous melt extraction and weak refertilization of mantle peridotites at the Vema lithospheric section (Mid-Atlantic Ridge). *Journal of Petrology* **7**, 745–71.

BURKE, K. 1988. Tectonic evolution of the Caribbean. *Annual Review of Earth and Planetary Sciences* **16**, 201–30.

BURKE, K., FOX, P. G. & ŞENGŐR, A. M. C. 1978. Buoyant ocean floor and the origin of the Caribbean. *Journal of Geophysical Research* **83**, 3949–54.

CASEY, J. F. & DEWEY, J. F. 1984. Initiation of subduction zones along transform and accreting plate boundaries, triple-junction evolution, and forearc spreading centres—implications for ophiolitic geology and obduction. In *Ophiolites and Oceanic Lithosphere* (eds I. G. Gass, S. J. Lippard & A. W. Shelton), pp. 269–90. Geological Society of London, Special Publication no. 13.

CHAUVEL, C. & BLICHERT-TOFT, J. 2001. A hafnium isotope and trace element perspective on melting of the depleted mantle. *Earth and Planetary Science Letters* **90**, 137–51.

CHOI, S. H., MUKASA, S. B., ANDRONIKOV, A. V. & MARCANO, M. C. 2007. Extreme Sr-Nd-Pb-Hf isotopic compositions exhibited by the Tinaquillo peridotite massif, Northern Venezuela: implications for geodynamic setting. *Contributions to Mineralogy and Petrology* **153**, 443–63.

CHOI, S. H., MUKASA, S. B. & SHERVAIS, J. W. 2008. Initiation of Franciscan subduction along large-offset fracture zone: Evidence from mantle peridotites, Stonyford, California. *Geology* **36**(8), 595–98.

CHOI, S. H., MUKASA, S. B., ZHOU, X. H., XIAN, X. H. & ANDRONIKOV, A. V. 2008. Mantle dynamics beneath East Asia constrained by Sr, Nd, Pb and Hf isotopic systematics of ultramafic xenoliths and their host basalts from Hannuoba, North China. *Chemical Geology* **248**, 40–61.

COLEMAN, R. G. 1977. *Ophiolites: Ancient Oceanic Lithosphere?* Berlin, Heidelberg, New York: Springer Verlag, 229 pp.

COX, D. P., MARVIN, R. F., M'GONIGLE, J. W., MCINTYRE, D. H. & ROGERS, C. L. 1977. Potassium–argon geochronology of some metamorphic, igneous, and hydrothermal events in Puerto Rico and the Virgin Islands. *US Geological Survey Journal of Research* **5**, 689–703.

DEBAILLE, V., BLICHERT-TOFT, J., AGRANIER, A., DOUCELANCE, R., SCHIANO, P. & ALBARÈDE, F. 2006. Geochemical component relationship in MORB from the Mid-Atlantic Ridge, 22–35° N. *Earth and Planetary Science Letters* **241**, 884–62.

DENYER, P. & GAZEL, E. 2009. The Costa Rican Jurassic to Miocene oceanic complexes: Origin, tectonics and relations. *Journal of South American Earth Sciences* **28**, 429–42.

DICK, H. J. B. & BULLEN, T. 1984. Chromian spinel as a petrogenetic indicator in abyssal and alpine-type peridotites and spatially associated lavas. *Contributions to Mineralogy and Petrology* **86**, 54–76.

DILEK, Y., MOORES, E., ELTHIN, D. & NICOLAS, A. 2000. *Ophiolites and Oceanic Crust: New Insights from Field Studies and the Ocean Drilling Program*. Boulder, CO: Geological Society of America.

DONNELLY, T. W. 1985. Mesozoic and Cenozoic plate evolution of the Caribbean region. In *The Great American Biotic Interchange* (eds F. G. Stehli & S. D. Webb), pp. 89–121. New York: Springer.

DOSTAL, J., DUPUY, C. & PUDOIGNON, P. 1996. Distribution of boron, lithium and beryllium in ocean island basalts from French Polynesia: implications for the B/Be and Li/Be ratios as tracers of subducted components. *Mineralogical Magazine* **60**, 563–80.

DUNCAN, R. A. & HARGRAVES, R. B. 1984. Plate tectonic evolution of the Caribbean region in the mantle reference frame. In *The Caribbean–South American Plate Boundary and Regional Tectonics* (eds W. E. Bonini, R. B. Hargraves & R. Shagam), pp. 81–93. Geological Society of America, Memoir no. 162.

EGGINS, S. M., RUDNICK, R. L. & MCDONOUGH, W. F. 1998. The composition of peridotites and their minerals: a laser-ablation ICP-MS study. *Earth and Planetary Science Letters* **154**, 53–71.

ESCUDER-VIRUETE, J., CASTILLO-CARRION, M. & PEREZ-ESTAUN, A. 2014. Magmatic relationships between depleted mantle harzburgites, boninitic cumulate gabbros and subduction-related tholeiitic basalts in Puerto Plata ophiolitic complex, Dominican Republic: Implications for the birth of the Caribbean island-arc. *Lithos* **196–197**, 261–80.

FREY, F. A., GREEN, D. H. & ROY, S. D. 1978. Integrated models of basalt petrogenesis: a study of quartz tholeiites to olivine melilitites from South Eastern Australia utilizing geochemical and experimental petrological data. *Journal of Petrology* **19**, 463–513.

GAZEL, E., ABBOTT, JR. R. N. & DRAPER, G. 2011. Garnet-bearing ultramafic rocks from the Dominican Republic: Fossil mantle plume fragments in an ultra high pressure oceanic complex? *Lithos* **125**, 393–404.

GELDMACHER, J., HANAN, B. B., BLICHERT-TOFT, J., HARPP, K., HOERNLE, K., HAUFF, F., WERNER, R. & KERR, A. C. 2003. Hafnium isotopic variations in volcanic rocks from the Caribbean Large Igneous Province and Galápagos hot spot tracks. *Geochemistry, Geophysics, Geosystems*, published online 19 July 2003. doi: 10.1029/2002GC000477.

GHOSH, N., HALL, S. A. & CASEY, J. F. 1984. Seafloor spreading magnetic anomalies in the Venezuelan Basin. In *The Caribbean–South American Plate Boundary and Regional Tectonics* (eds W. Bonini, R. B. Hargraves & R. Shagam), pp. 54–80. Geological Society of America, Memoir no. 162.

GIUNTA, G., BECCALUVA, L., COLTORTI, M., MORTELLARO, D. & SIENA, F. 2002. The peri-Caribbean ophiolites: structure, tectono-magmatic significance and geodynamic implications. *Caribbean Journal of Earth Science* **36**, 1–20.

HAMLYN, P. R. & BONATTI, E. 1980. Petrology of mantle-derived ultramafics from the Owen fracture, northwest Indian Ocean: Implications for the nature of the oceanic upper mantle. *Earth and Planetary Science Letters* **48**, 65–79.

HART, S. R. 1984. A large-scale isotope anomaly in the Southern Hemisphere mantle. *Nature* **309**, 753–57.

HART, S. R. & ZINDLER, A. 1986. In search of a bulk-Earth composition. *Chemical Geology* **57**, 247–67.

HASTIE, A. R., KERR, A., MITCHELL, S. & MILLAR, I. L. 2008. Geochemistry and petrogenesis of Cretaceous oceanic plateau lavas in eastern Jamaica. *Lithos* **101**, 323–43.

HAUFF, F., HOERNLE, K., TILTON, G., GRAHAM, D. W. & KERR, A. C. 2000. Large volume recycling of oceanic lithosphere over short time scales: geochemical constraints from the Caribbean Large Igneous Province. *Earth and Planetary Science Letters* **174**, 247–63.

HAUFF, F., HOERNLE, K., VAN DEN BOGAARD, P., ALVARADO, G. & GARBE-SCHÖNBERG, D. 1999. Age and geochemistry of basaltic complexes in western Costa Rica: Contributions to the geotectonic evolution of Central America. *Geochemistry, Geophysics, Geosystems*, published online 30 May 2000. doi: 10.1029/1999GC000020.

HELLEBRAND, E., SNOW, J. E., DICK, H. J. B. & HOFMANN, A. W. 2001. Coupled major and trace elements as indicators of the extent of melting in mid-ocean-ridge peridotites. *Nature* **410**, 677–81.

HELLEBRAND, E., SNOW, J. E. & MÜHE, R. 2002. Mantle melting beneath Gakkel Ridge (Artic Ocean): abyssal peridotite spinel compositions. *Chemical Geology* **182**, 227–35.

HERZBERG, C. & GAZEL, E. 2009. Petrological evidence for secular cooling in mantle plumes. *Nature* **458**, 619–22.

HESS, H. H. & OTALORA, G. 1964. Mineralogical and chemical composition of the Mayaguez serpentinite cores. In *A Study of Serpentinite: The AMSOC Core Hole near Mayaguez, Puerto Rico* (ed. C. A. Burk), pp. 152–69. Washington, DC: National Academy of Science NSF Pub.

ITO, E., WHITE, W. & GOPEL, C. 1987. The O, Sr, Nd and Pb isotope geochemistry of MORB. *Chemical Geology* **62**, 157–76.

JAGOUTZ, E., PALME, H., BLUM, H., CENDALES, M., DREIBUS, G., SPETTEL, B., LORENZ, V. & WANKE, H. 1979. The abundances of major, minor and trace elements in the Earth's mantle as derived from primitive ultramafic nodules. In *Proceedings of 10th Lunar Planetary Science Conference* **2**, 2031–50. New York: Pergamon Press.

JANSMA, P. E., MATTIOLI, G. S., LOPEZ, A., DEMETS, C., DIXON, T. H., MANN, P. & CALAIS, E. 2000. Neotectonics of Puerto Rico and the Virgin Islands, northeastern Caribbean, from GPS geodesy. *Tectonics* **19**, 1021–37.

JOLLY, W. T., LIDIAK, E. G. & DICKIN, A. P. 2008*a*. The case for persistent southwest-dipping Cretaceous convergence in the northeast Antilles: geochemistry, melting models, and tectonic implications. *Geological Society of America Bulletin* **120**, 1036–52.

JOLLY, W. T., LIDIAK, E. G. & DICKIN, A. P. 2008*b*. Bimodal volcanism in northeast Puerto Rico and the Virgin Islands (Greater Antilles Island Arc): genetic link with Cretaceous subduction of the mid-Atlantic ridge Caribbean spur. *Lithos* **103**, 393–414.

JOLLY, W. T., LIDIAK, E. G., SCHELLEKENS, J. H. & SANTOS, H. 1998. Volcanism, tectonics, and stratigraphy correlations in Puerto Rico. *Geological Society of America* **322**, 1–34.

JOLLY, W. T., SCHELLEKENS, J. H. & DICKIN, A. P. 2007. High-Mg andesites and related lavas from the southwest Puerto Rico (Greater Antilles Island Arc): Petrogenic links with emplacement of the Late Cretaceous Caribbean mantle plume. *Lithos* **98**, 1–26.

KARSON, J. A., CANNAT, M., MILLER, D. J. & ELTHON, D. 1997. Mid-Atlantic Ridge: Leg 153, Sites 920–924. In *Proceedings of the Ocean Drilling Program, Scientific Results*. Oceanic Drilling Program no. 153, 577 pp.

KEMPTON, P. D., FITTON, J. G., SAUNDERS, A. D., NOWEL, G. M., TAYLOR, R. N., HARDARSON, B. S. & PEARSON, G. 2000. The Iceland plume in space and time: a Sr–Nd–Pb–Hf study of the North Atlantic rifted margin. *Earth and Planetary Science Letters* **177**, 255–71.

KERR, A. C. & TARNEY, J. 2005. Tectonic evolution of the Caribbean and northwestern South America: The case for accretion of two late Cretaceous oceanic plateaus. *Geology* **33**, 269–72.

KOGISO, T., TATSUMI, Y. & NAKANO, S. 1997. Trace element transport during dehydration processes in the subducted oceanic crust: 1. experiments and implications for the origin of ocean island basalts. *Earth and Planetary Science Letters* **148**, 193–205.

KÖHLER, T. P. & BREY, G. P. 1990. Calcium exchange between olivine and clinopyroxene calibrated as a geothermobarometer for natural peridotites from 2 to 60 kb with applications. *Geochimica et Cosmochimica Acta* **54**, 2375–88.

LAÓ-DÁVILA, D. A. 2014. Collisional zones in Puerto Rico and the northern Caribbean. *Journal of South American Earth Sciences* **54**, 1–19.

LAÓ-DÁVILA, D. A., LLERNADI-ROMÁN, P. A. & ANDERSON, T. H. 2012. Cretaceous–Paleogene thrust emplacement of serpentinite in southwestern Puerto Rico. *Geological Society of America Bulletin* **124**, 1169–90.

LE MAITRE, R. W., BATEMAN, P., DUDEK, A., KELLER, J., LAMEYRE LE BAS, M. J., SABINE, P. A., SCHMID, R., SORENSEN, H., STRECKEISEN, A., WOOLLEY, A. R. & ZANETTIN, B. (eds) 1989. *A Classification of Igneous Rocks and Glossary of Terms*. Oxford: Blackwell.

LIDIAK, E. G., JOLLY, W. T. & DICKIN, A. P. 2011. Pre-arc basement complex and overlying island arc strata, Southwestern Puerto Rico: overview, geologic evolution, and revised data bases. *Geological Acta* **9**, 273–87.

MADRIGAL, P., GAZEL, E., DENYER, P., SMITH, I., JICHA, B., FLORES, K. E., COLEMAN, D. & SNOW, J. 2015. A melt-focusing zone in the lithospheric mantle preserved in the Santa Elena Ophiolite, Costa Rica. *Lithos* **230**, 189–205.

MAHONEY, J. J., SINTON, J. M., KURZ, M. D., MACDOUGALL, J. D., SPENCER, K. J. & LUGMAIR, G. W. 1994. Isotope and trace element characteristics of a super-fast spreading ridge: East Pacific rise, 13–23° S. *Earth and Planetary Science Letters* **121**, 173–93.

MAMBERTI, M., LAPIERRE, H., BOSCH, D., JAILLARD, E., ETHIEN, R., HERNANDEZ, J. & POLVE, M. 2003. Accreted fragments of the Late Cretaceous Caribbean–Colombian Plateau in Ecuador. *Lithos* **66**, 173–99.

MARCHESI, C., JOLLY, W. T., LEWIS, J. F., GARRIDO, C. J., PROENZA, J. A. & LIDIAK, E. G. 2011. Petrogenesis of fertile mantle peridotites from the Monte del Estado Massif (Southwest Puerto Rico): a preserved section of Proto-Caribbean lithospheric mantle? *Geological Acta* **9**, 286–306.

MATTSON, P. H. 1960. Geology of the Mayagüez area, Puerto Rico. *Geological Society of America Bulletin* **71**, 319–62.

MATTSON, P. H. & PESSAGNO JR, E. A. 1979. Jurassic and early Cretaceous radiolarians in Puerto Rican ophiolite-tectonic implications. *Geology* **7**, 440–4.

MESCHEDE, M. & FRISCH, W. 1998. A plate-tectonic model for the Mesozoic and Early Cenozoic history of the Caribbean plate. *Tectonophysics* **296**, 269–91.

MONTGOMERY, H. M., PESSAGNO, E. A. JR. & PINDELL, J. L. 1994. A 195 Ma terrane in a 165 Ma sea: Pacific origin of the Caribbean plate. *Geological Society of America Today* **4**, 1–6.

MUKASA, S. B., SHERVAIS, J. W., WILSHIRE, H. G. & NIELSON, J. E. 1991. Intrinsic Nd, Pb, and Sr isotopic heterogeneities exhibited by the Lherz alpine peridotite massif, French Pyrenees. *Journal of Petrology*, Special Lherzolite Issue, 117–34.

MÜNKER, C., WEYER, S., SCHERER, E. & MEZGER, K. 2001. Separation of high field strength elements (Nb, Ta, Zr, Hf) and Lu from rock samples for MC-ICPMS measurements. *Geochemistry, Geophysics,*

Geosystems, published online 14 December 2001. doi: 10.1029/2001GC000183.

NICKEL, K. G. 1986. Phase-equilibria in the system SiO_2–MgO–Al_2O_3–CaO–Cr_2O_3 (SMACCR) and their bearing on spinel/garnet lherzolite relationships. *Neues Jahrbuch Fur Mineralogie-Abhandlunge* **155**, 259–87.

NIU, Y., COLLERSON, K. D., BATIZA, R., IMMO, J. & REGELOUS, M. 1999. Origin of enriched-type mid-ocean basalt at ridges far from mantle plumes: The East Pacific Rise at 11° 20′ N. *Journal of Geophysical Research* **104**, 7067–87.

NOWELL, G. M., KEMPTON, P. D., NOBLE, S. R., FITTON, J. G., SAUNDERS, A. D., MAHONEY, J. J. & TAYLOR, R. N. 1998. High precision Hf isotope measurements of MORB and OIB by thermal ionization mass spectrometry: insights into the depleted mantle. *Chemical Geology* **149**, 211–33.

PARLAK, O., HÖCK, V., KOZLU, H. & DELALOYE, M. 2004. Oceanic crust generation in an island arc tectonic setting, SE Anatolian orogenic belt (Turkey). *Geological Magazine* **141**, 583–603.

PEARCE, J. A., ALABASTER, T., SHELTON, A. W. & SEARLE, M. P. 1981. The Oman ophiolite as a Cretaceous arc-basin complex: evidence and implications. *Philosophical Transactions of the Royal Society of London* **A300**, 299–317.

PEARSON, D. G., CANIL, D. & SHIREY, S. B. 2004. Mantle samples included in volcanic rocks: xenoliths and diamonds. In *The Mantle and Core* (R.W. Carlson), pp. 171–275. Elsevier, Treatise on Geochemistry, Volume 2.

PEARCE, J. A. & CANN, J. R. 1973. Tectonic setting of basic volcanic rocks determined using trace element analyses. *Earth and Planetary Science Letters* **19**, 290–300.

PEARCE, J. A. & NORRY, M. J. 1979. Petrogenetic implications of Ti, Zr, Y, and Nb variations in volcanic rocks. *Contributions to Mineralogy and Petrology* **69**, 33–47.

PEARCE, J. A. & PEATE, D. W. 1995. Tectonic implications of the composition of volcanic arc magmas. *Annual Review of Earth and Planetary Sciences* **23**, 281–85.

PINDELL, J. L. & BARRETT, S. F. 1990. Geological evolution of the Caribbean region: a plate tectonic perspective. In *The Caribbean Region* (eds G. Dengo & J. E. Case), pp. 405–32. Geological Society of America, Geology of North America, Vol. H.

PINDELL, J. L., KENNAN, L., MARESCH, W. V., STANEK, K.-P., DRAPER, G. & HIGGS, R. 2005. Plate-kinematics and crustal dynamics of circum-Caribbean arc-continent interactions: Tectonic controls on basin development in Proto-Caribbean margins. In *Caribbean-South American Plate Interactions, Venezuela* (eds H. G. A. Lallemant & V. B. Sisson), pp. 7–52. Geological Society of America, Special Paper no.394.

PINDELL, J., MARESCH, W. V., MARTENS, U. & STANEK, K. 2012. The Greater Antillean Arc: Early Cretaceous origin and proposed relationship to Central American subduction mélanges: implications for models of Caribbean evolution. *International Geology Review* **54**, 131–43.

REID, I. & JACKSON, H. R. 1981. Oceanic spreading rate and crustal thickness. *Marine Geophysical Research* **5**, 165–72.

ROEHRIG, E. E., LAÓ-DÁVILA, D. A. & WOLFE, A. L. 2015. Serpentinization history of the Río Guanajibo serpentinite body, Puerto Rico. *Journal of South American Earth Sciences* **62**, 195–217.

SALTERS, V. J. M. & WHITE, W. M. 1998. Hf isotope constraints on mantle evolution. *Chemical Geology* **145**, 447–60.

SCHELLEKENS, J. H. 1998*a*. Geochemical evolution and tectonic history of Puerto Rico. In *Tectonics and Geochemistry of the Northeastern Carribean* (eds E. G. Lidiak & D. K. Larue), pp. 35–66. Geological Society of America, Special Papers no. 322.

SCHELLEKENS, J. H. 1998*b*. Composition, metamorphism grade, and origin of metabasites in the Bermeja Complex, Puerto Rico. *International Geology Review* **40**, 722–47.

SHERVAIS, J. W. 2001. Birth, death, and resurrection: the life cycle of suprasubduction zone ophiolites. *Geochemistry, Geophysics, Geosystems*, published online 31 January 2001. doi: 10.1029/2000GC000080.

SINTON, C. W., DUNCAN, R. A., STOREY, M., LEWIS, J. & ESTRADA, J. J. 1998. An oceanic flood basalt province within the Caribbean plate. *Earth and Planetary Science Letters* **155**, 221–35.

SMITH, A. & SCHELLEKENS, J. H. 1998. Batholiths as markers of tectonic change in the northeastern Caribbean. In *Tectonics and Geochemistry of the Northeastern Carribean* (eds E. G. Lidiak & D. K. Larue), pp. 99–121. Geological Society of America, Special Papers no. 322.

STERN, R. J. & BLOOMER, S. H. 1992. Subduction zone infancy: Examples from the Eocene Izu-Bonin-Mariana and Jurassic California arcs. *Geological Society of America Bulletin* **104**, 1621–36.

SUN, S. S. & MCDONOUGH, W. F. 1989. Chemical and isotopic systematics of oceanic basalts: implications for mantle composition and process. In *Magmatism in the Ocean Basins* (eds A. D. Saunders & M. J. Norry), pp. 313–45. Geological Society of London, Special Publication no. 42.

THOMPSON, P. M. E., KEMPTON, P. D., WHITE, R. V., KERR, A. C., TARNEY, J., SAUNDERS, A. D., FITTON, J. G. & MCBIRNEY, A. 2003. Hf–Nd isotope constraints on the origin of the Cretaceous Caribbean plateau and its relationship to the Galápagos plume. *Earth and Planetary Science Letters* **217**, 59–75.

VEIZER, J. 1989. Sr isotopes in seawater through time. *Annual Review of Earth Planetary Sciences* **17**, 141–67.

VOLCKMANN, R. P. 1984. Geologic map of the Puerto Real Quadrangle, Southwest Puerto Rico. In *Miscellaneous Investigations Series*, Map I-1559, scale 1:20,000. United States Geological Survey.

WAKABAYASHI, J. & DILEK, Y. 2003. What constitutes 'emplacement' of an ophiolite? Mechanisms and relationship to subduction initiation and formation of metamorphic soles. In Ophiolites in Earth History (eds Y. Dilek & R. T. Robinson), pp. 427–47. Geological Society of London, Special Publication no. 218.

WALKER, R. J., STOREY, M., KERR, A.C., TARNEY, J. & ARNDT, N. T. 1999. Implications of ^{187}Os isotopic heterogeneities in a mantle plume: Evidence from Gorgona Island and Curaçao. *Geochimica et Cosmochimica Acta* **63**, 713–28.

WÄNKE, H. 1981. Constitution of terrestrial planets. *Philosophical Transactions of the Royal Society of London, A* **303**, 287–302.

WEBB, S. A. C. & WOOD, B. J. 1986. Spinel–pyroxene–garnet relationships and their dependence on Cr/Al ratio. *Contributions to Mineralogy and Petrology* **92**, 471–80.

WELLS, P. R. A. 1977. Pyroxene thermometry in simple and complex systems. *Contributions to Mineralogy and Petrology* **62**, 129–39.

WHITE, W. M. & PATCHETT, P. J. 1984. Hf–Nd–Sr isotopes and incompatible element abundances in island arcs: implications for magma origins and crust–mantle evolution. *Earth and Planetary Science Letters* **67**, 167–85.

WHITE, R. V., TARNEY, J., KERR, A. C., SAUNDERS, A. D., KEMPTON, P. D., PRINGLE, M. S. & KLAVER, G. T. 1999. Modification of an oceanic plateau, Aruba, Dutch Caribbean: Implications for the generation of continental crust. *Lithos* **46**, 43–68.

WILKINSON, J. F. G. & LE MAITRE, R. W. 1987. Upper mantle amphiboles and micas and TiO_2, K_2O, and P_2O_5 abundances and 100 $Mg/(Mg + Fe^{2+})$ ratios of common basalts and andesites: Implications for modal mantle metasomatism and undepleted mantle compositions. *Journal of Petrology* **28**, 37–73.

https://doi.org/10.1017/S001675681500093X Published online by Cambridge University Press